

8. PETROGRAPHIC CONTRIBUTIONS TO THE INVESTIGATION OF VOLCANICLASTIC SEDIMENTS IN THE WESTERN WOODLARK BASIN, SOUTHWEST PACIFIC (ODP LEG 180)¹

Luciano Cortesogno,² Laura Gaggero,² and Stefania Gerbaudo²

ABSTRACT

This report includes the petrographic description and reviews the distribution of lithic clasts in sediments drilled during Leg 180 in the Woodlark Basin (southwest Pacific). The lithic clasts include (1) metamorphic rocks; (2) granites; (3) serpentinites, gabbros, dolerites, and basalts likely derived from the Papuan ophiolite belt; (4) rare alkaline volcanites reworked in middle Miocene sediments; (5) medium- to high-K calc-alkaline island arc volcanites, in part as reworked clasts, and explosive products deposited by fallout or reworked by turbiditic currents; and (6) rare sedimentary fragments.

At the footwall sites the clast assemblage evidences the association of dolerites and evolved gabbroic rocks; the serpentinite likely pertaining to the same ophiolitic complex are likely derived from onland outcrops and transported by means of turbidity currents. On the whole, extensional tectonics active at least since the middle Pliocene can be inferred.

The calc-alkaline volcanism is in continuity with the arc-related products from the Papua Peninsula and D'Entrecasteaux Islands and with the latest volcanics of the Miocene Trobrian arc. However, the medium- to high-K and shoshonitic products do not display a significant temporal evolution within the stratigraphic setting. Lava clasts, volcanogenic grains, and glass shards are associated with turbidity currents, whereas in the Pliocene of northern margin the increasing frequency of

¹Cortesogno, L., Gaggero, L., and Gerbaudo, S., 2001. Petrographic contributions to the investigation of volcanoclastic sediments in the western Woodlark Basin, southwest Pacific (ODP Leg 180). In Huchon, P., Taylor, B., and Klaus, A. (Eds.), *Proc. ODP, Sci. Results*, 180, 1–44 [Online]. Available from World Wide Web: <http://www-odp.tamu.edu/publications/180_SR/VOLUME/CHAPTERS/159.PDF>. [Cited YYYY-MM-DD]

²Dipartimento per lo Studio del Territorio e delle sue Risorse, Università degli Studi di Genova, Italy. Correspondence author: gerbaudo@box.tin.it; gerbaudo@dipteris.unige.it; and gerbaudo@noos.fr

Initial receipt: 3 January 2001
Acceptance: 22 June 2001
Web publication: 2 November 2001
Ms 180SR-159

tephra (glass shards and vesicular silicic fragments) suggests more explosive activity and increasing contribution to the sediments from aerial fallout materials.

Evidence of localized alkalic volcanism of presumable early to middle Miocene age is a new finding. It could represent a rift phase earlier than or coeval to the first opening of the Woodlark Basin or, less probably, could derive from depositional trajectories diverted from an adjacent basin.

INTRODUCTION

During Leg 180 the record of continental rifting evolving to seafloor spreading in the region of Papua New Guinea was documented (Fig. F1). A roughly north-south transect of 11 holes was drilled across the Woodlark rift basin from the footwall to the downflexed northern margin of the rift. During this leg, the tectonic-sedimentary history and rifting processes were revealed from late Miocene to Holocene time as a backarc basin related to subduction (Shipboard Scientific Party, 1999).

The most significant contribution concerns the modeling of a complete lithospheric extension. Seafloor magnetic anomalies show that most of the rifting occurred during the last 6–8 m.y., starting in an eastward extension of the Papuan Peninsula as a westward-propagating spreading center that opened the Woodlark Basin (Weissel et al., 1982; Taylor et al., 1995; Goodliffe et al., 1997; Goodliffe, 1998).

This chapter addresses the petrography of sandstones and epiclastites from the clastic and volcanoclastic units drilled during Ocean Drilling Program Leg 180 from the northern margin throughout the rift basin sites to the footwall. In particular, investigations of metamorphic, igneous intrusive, and volcanic clasts give insights into the relationships between phases of tectonic uplift, consequent erosion of deep material, and episodes of volcanic activity during the evolution of different sectors of the basin.

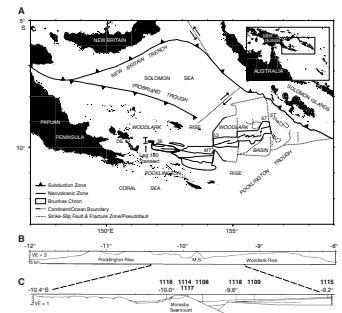
MATERIALS AND METHODS

Investigations were conducted on 603 samples from a shipboard sampling program specifically designed to address sedimentary textures and petrography of the 31 units at Sites 1115, 1109, and 1118 (northern margin), four units at Site 1108 (footwall), and 10 units at Sites 1114 and 1116 (rift basin) (Fig. F1).

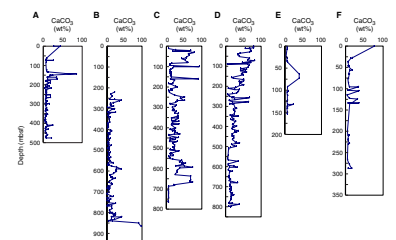
Petrographic analysis by means of optical microscopy was carried out on 54 samples and on the whole set of 232 shipboard thin sections for a total of 181 specimens from the northern margin sites, 51 in the rift basin sites, and 54 from the footwall sites. All 603 samples investigated underwent calcimetric analysis on the fine-grained (silty/clay) component (Fig. F2), 80 underwent X-ray diffraction (XRD) analysis, and 25 clay analyses were performed on separates. Calcimetry was performed using the “Dietrich-Fruhling” calcimeter. The method is based on the measurement of CO₂ volume developed by acid reacting with the powdered rock. The total carbonate present is obtained using formulae that take into account the pressure, temperature, amount of previously weighed sediment, and the volume of CO₂ developed.

XRD analyses were carried out using a Philips PW3710 diffractometer at the University of Genova, Italy. Samples were run between 2.5° and

F1. Major physiographic features and active plate boundaries of the Woodlark Basin region, p. 16



F2. Downhole CaCO₃, p. 17.



70°2 θ , with a generator potential of 30 kV, a generator current of 22 mA (using CuK α radiation), a Ni filter, and a scan speed of 1°/min. The software used for XRD data reduction was Philips PC-APD diffraction software. Clay minerals were determined by XRD analyses, including measurements of air-dried and glycolated powder mounts.

Some samples, previously studied under the light microscope, were selected for the quantification of total organic carbon using a Carlo Erba CHNS-O EA1110 elemental analyzer before (total C) and after (organic C) removal of carbonates by HCl addition (Hedges and Stern, 1984). Cyclohexanone 2,4-dinitrophenylhydrazone was used as a standard. Instrumental detection limits are 0.5 μ g for both C and N. The variation coefficient for instrumental bias is given as 0.8% for C and 1.3% for N.

Twenty-six samples were selected for study by electron microprobe, with particular attention to the occurrence of coarse-grained rock fragments. These analyses characterized representative compositions of mineral phases in igneous and metamorphic clasts; glass shards were also analyzed for major oxide components. The analyses were performed by a SEM-EDS microprobe at the University of Genova, equipped with an X-ray dispersive analyzer (EDAX PV9100). Operating parameters were 15-kV accelerating voltage, 2.20-nA beam current, and 1- to 10- μ m beam diameter (up to 25 μ m for the glass and clay minerals). Natural silicate standards were used (Na: tremolite [0.5 wt%], pargasite [2.30 wt%], albite [11.81 wt%]; Mg: forsterite [57.22 wt%]; Al: K-anorthoclase [20.12 wt%]; Si: diopside [55.12 wt%]; K: microcline [16.09 wt%]; Ca: clinopyroxene [17.22 wt%]; Ti: ilmenite [45.70 wt%]; Mn: rhodonite [45.15 wt%]; Fe: fayalite [67.54 wt%]; Cr: garnet [1.56 wt%]). Na $_2$ O and MgO contents analyzed in silicates by means of an EDAX microprobe are generally underestimated if the analysis is processed with current automatic methods. To overcome this problem, the background for Na (1.040 keV) and Mg (1.252 keV) was manually corrected to range between 0.9 and 4.2 keV.

Orthopyroxene and clinopyroxene analyses were calculated according to the stoichiometric method of simultaneous balancing to 4.00 cations and 6.00 oxygens. End-members were calculated in the following sequence: wollastonite, enstatite, ferrosilite, aegirine, jadeite, CaAl $_2$ SiO $_6$, CaFeAlSiO $_6$, CaCrAlSiO $_6$, and CaTiAl $_2$ O $_6$. Morimoto et al. (1988) and Rock (1990) nomenclatures were adopted.

The Ca amphiboles cation sum was balanced to 13-(Ca+Na+K), Fe $^{3+}$ = 46 total cation charge, Fe $^{2+}$ = Fe $_{tot}$ - Fe $^{3+}$, Al IV = 8 - Si, and Al IV = Al $_{tot}$ - Al V . Rock and Leake (1984) nomenclature was adopted.

Plagioclase analyses, on the basis of eight oxygens, were recalculated to total cations = 5. Ilmenites were recast on the basis of three oxygens. Magnetites and Ti magnetites were recast on the basis of four oxygens.

LITHOLOGY

The lithologic features, based on thin section studies, are summarized in Tables T1, T2, T3, T4, and T5. The silicoclastic samples were classified on the grounds of clast/matrix ratio and clast size. The nature of the lithic clasts is reported, together with bioclasts, organic matter occurrence, the description of matrix or cement, the presence of sedimentary structures, grain size, roundness and sorting of grains, and evidence of alteration.

T1. Petrographic features of sediments from footwall sites, p. 22.

T2. Petrographic features of sediments from rift basin sites, p. 24.

T3. Petrographic features of sediments from northern margin Site 1109, p. 26.

T4. Petrographic features of sediments from northern margin Site 1115, p. 28.

T5. Petrographic features of sediments from northern margin Site 1118, p. 30.

MESOSCOPIC SEDIMENTARY STRUCTURES

At all sites, the most common sedimentary structures are parallel laminations in the fine-grained facies, together with interbedding between fine-grained sediments and sandstones observed both at meso- and microscales (Pl. P1, figs. 4, 5).

As also pointed out by the Shipboard Scientific Party (1999), sedimentary structures evidently linked to sediment remobilization by turbidity currents are very common in Holes 1108B and 1116A. In particular in some sandstones, high-angle tabular cross-lamination is present (Cores 180-1108B-9R and 10R) and classic Bouma (Bouma, 1962) sequences are prominent features (e.g., interval 180-1108B-24R-2, 4–36 cm) (Pl. P1, fig. 6). In Hole 1116A, cross and convolute laminations in claystones and siltstones (Cores 180-1116A-1R through 4R) and in fine- to medium-grained sandstones (Cores 180-1116A-9R through 18R) are locally present. Normal grading in sandstones is common in Hole 1108B and reverse grading also occurs. The presence in Holes 1108B and 1116A of so many structures linked to turbidity currents is probably due to destabilization of still unconsolidated sediments coming from Moresby Seamount (Pl. P1, fig. 2). Moreover, intraformational rip-up clasts at these sites indicate the presence of high-energy currents, which remobilized newly deposited sediment. On the other hand, low-angle cross-laminations and graded beds present locally in silty sandstones in Hole 1115C (Cores 180-1115C-15R through 20R) are probably linked to marginal bottom currents. Bioturbation is common, especially in clayey siltstones at the rift basin (Cores 180-1108B-16R through 21R) and in claystones at the northern margin sites (Cores 180-1115C-1R through 11R and Cores 180-1109C-10H through 39X).

PETROLOGY

Matrix

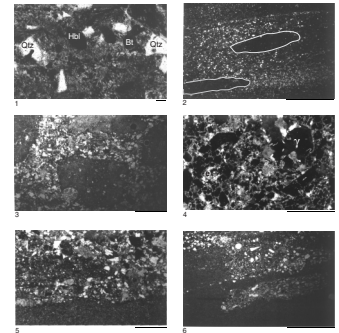
In the thin sections studied, arenite matrix varies from calcareous-argillaceous matrix by the common presence of volcaniclastic glass to essentially glassy texture. The fundamental constituents identified by matrix analysis are listed in Table T6. Alteration of the glassy component produced clay minerals, such as saponite, talc, and chlorite (Table T7). Clay minerals from terrigenous detrital components are probably also present in the matrix; planktonic foraminifers, benthic foraminifers, and small shell fragments are also locally abundant.

As a general feature, the abundance of volcaniclastic supplies tends to decrease the carbonate rate (Pl. P1, fig. 4).

Biogenic Components and Bioclasts

Planktonic and benthic foraminifers that show different degrees of test preservation were observed at all sites. Subangular to subrounded bioclasts appear regularly and are generally easily recognizable. In particular, as revealed in the thin sections studied, mollusc fragments are common in the northern margin sites (Holes 1109C, 1109D, 1115C, and 1118A). A few bryzoan fragments were found in Hole 1108B between 14.5 and 226.79 meters below seafloor (mbsf). Bryozoans occur in calcareous fine-grained sediments or packstones at Site 1109 (intervals 180-1109C-21X-CC, 40–42 cm; 180-1109D-32R-2, 101–103 cm;

P1. Photomicrographs of representative structures, p. 41.



T6. Mineral compositions of arenitic siltitic sediment matrix, p. 32.

T7. Clay mineral composition of mud matrix samples, p. 34.

and 180-1109D-36R-6, 51–54 cm), Site 1115 (intervals 180-1115C-23R-1, 93–94 cm, and 33R-3, 68–71 cm), and in Hole 1118A between 853.87 and 868.7 mbsf. In the same interval in Hole 1118A, coral and calcareous red algal fragments are also present. Red algal fragments were found also in Hole 1108B (interval 180-1108B-31R-2, 20.5–23.5 cm), in Hole 1115C between 566.83 and 648.11 mbsf, and in conglomerate in Hole 1116A (interval 180-1116A-6R-1, 9–11 cm). A large coral fragment is also present in Hole 1109C (interval 180-1109C-24X-CC, 18–20 cm). Ostracode shells are very rare and are found only in Hole 1108A (intervals 180-1108B-22R-4, 61–64 cm, and 28R-3, 28–31 cm).

Total Organic Carbon

The organic carbon content is generally very low to absent in most sandstones, but concentrations are present in fine-grained siltstones and claystones. Some samples were analyzed for organic carbon on the grounds of its presence as scant patches at all sites, as ribbons (Site 1108 at 448.16 mbsf, Site 1112 between 1.7 and 20.52 mbsf, Site 1114 at 36.04 mbsf, Site 1116 at 8 mbsf, and Hole 1109D between 697.1 and 708.68 mbsf), or localized within foraminifer tests (Samples 180-1115C-15R-3, 79–83 cm, and 180-1118A-69R-3, 58–61 cm). The N content is negligible or below the method detection limits, whereas the C content is as much as 15.01 wt% (Table T8).

Carbonates

The total carbonate data shown in Figure F2 was integrated with XRD determination of mineral phases (Table T6). The predominant phase is calcite followed by aragonite, restricted to some samples at Sites 1109 and 1118, and dolomite (Samples 180-1109C-27X-4, 67–71 cm; 180-1109D-4R-5, 59–62 cm; 180-1109D-36R-6, 51–54 cm; and 180-1118A-39R-3, 100–103 cm). In two samples, ankerite was also found (Samples 180-1109D-34R-1, 10–13 cm, and 180-1115B-10H-4, 55–61.5 cm). The carbonates largely relate to shells and skeletal structures of organisms (also fragmentary bioclasts) and to the finest portion of the rock (matrix) because of either an organic or biochemical origin. The abundance of volcanoclastic supplies tends to decrease the carbonate rate.

Middle Miocene sediments in Hole 1115 usually have low carbonate contents. Average values increase significantly in the upper Miocene sequence. Pliocene turbiditic sedimentation is characterized by sharp variations in carbonate contents clearly linked to the nature and provenance of the turbidity currents.

Pelagic and hemipelagic Pleistocene sedimentation is characterized by highest carbonate values, consistent with the occurrence of nannofossil-rich silty clay (Sites 1108, 1114, and 1115). This can be related to the construction of a carbonate platform northwest of the Woodlark Rift (Robertson et al., in press).

Lithic Components

Metamorphic Lithic Clasts

Clasts of quartz-mica schists, gneisses, and amphibolites are present in the rift basin from the middle Pliocene (Site 1108) to the Pleistocene (Sites 1112). The fine grain size of mica schists and gneisses allows only

T8. Organic carbon content of pelite samples, p. 35.

a broad pertinence to amphibolite facies. The occurrence of muscovite in these sequences likely has the same significance. At the footwall, rare retrogressed amphibolites are found; amphibolite clasts are medium to fine grained with green hornblende and minor saussuritic plagioclase. The alteration of hornblende to actinolite is common and consistent with retrograde overprint to greenschist facies (Shipboard Scientific Party, 1999).

Pebbles and cobbles of mica schists, gneisses, and amphibolites, together with granites, were recovered from the talus at the foot of Moresby Seamount (Sites 1110 and 1113) (Shipboard Scientific Party, 1999).

Epidote ± chlorite clasts lacking schistosity at Site 1116 (0–20 mbsf), Site 1114 (200 mbsf), and Site 1108 (between 14 and 302 mbsf) likely derive from reworking of fracture-filling materials formed under greenschist/subgreenschist conditions. A fault gauge origin is likely also for talc schist, chlorite schist, and serpentine schist, which occur diffusely in the rift and footwall sites but are exceptionally rare in the northern margin sites.

Granite Clasts

Granites from footwall and rift-basin sites are microgranular with hypidiomorphic to granophyric texture (Pl. P2, fig. 3). They include plagioclase, K-feldspar, quartz, and biotite. Their nature and texture point to an origin from intrusions in the upper continental crust.

Serpentinite Clasts

Fragments (1–5 mm in size) of serpentinite showing mesh and ribbon textures, sometimes partially altered to talc and chlorite, and grains of Cr spinel ($Mg\# \approx 67$; $Cr/Cr+Al \approx 33$) represent evidence of eroded ultramafic mantle rocks (Pl. P2, fig. 2).

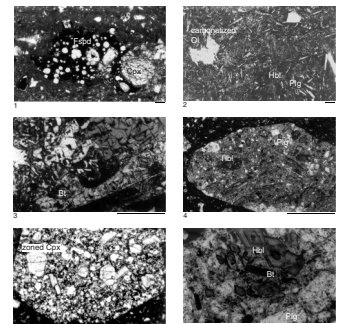
The spinels are very similar in color and composition (except for rare secondary ferric brown). The composition is consistent with spinels in poorly depleted lherzolites (Hoogerduijn Strating et al., 1990). Serpentinites and spinel grains are present at Site 1108 between the middle Pliocene–Pleistocene down to 332 mbsf and are diffuse throughout Hole 1116A. In the northern margin at Site 1115, rare spinel grains and rock fragments occur in upper Miocene sandstone (Sample 180-1115C-29R-1, 72.0–73.0 cm). The diffuse occurrence of serpentinite clasts throughout the sequences, as suggested by Shipboard Scientific Party (1999), was not confirmed.

Microgabbros, Diorites, and Metagabbro Clasts

Gabbroic clasts are present at the foot of Moresby Seamount at Site 1116 between 0.58 and 42.77 mbsf. In the rift basin, gabbros are rare (Sample 180-1108B-47R-1, 33.0–37.5 cm) and are doubtfully represented by sheared metagabbros at Site 1112. In the northern margin, clasts are present at Site 1115 in upper Miocene conglomerates and sandstones directly overlying the unconformity (Sample 180-1115C-30R-CC, 16.0–19.0 cm), and in Hole 1118A, gabbro occurs in middle Miocene conglomerate with prevalent dolerite clasts (Samples 180-1118A-71R-1, 13.0–15.0 cm, and 71R-1, 29.0–31.0 cm).

The grain size varies from medium to medium fine. One lithoclast (Sample 180-1108B-47R-1, 33–37.5 cm), showing mesh-textured ser-

P2. Photomicrographs of clast types, p. 42.



pentine and plagioclase (An_{75}), likely represents the only record of a cumulate olivine gabbro. More commonly, the clasts are Fe-Ti oxide gabbros (plagioclase $An \approx 70$, clinopyroxene, and ilmenite \pm rare olivine), Fe-Ti oxide diorites, and quartz diorites with clinopyroxene and hornblende as mafic silicates. On the whole, the mineral composition is consistent with the more evolved members of intrusive tholeiitic sequences.

In gabbroic clasts, actinolite diffusely replaces igneous mafic phases and chlorite and albite overgrow plagioclase. In Samples 180-1116A-6R-1, 9–11 cm, and 6R-1, 37–39 cm, gabbroic clasts show diffuse development of prehnite replacing plagioclase and filling veins (Pl. P3, fig. 1). Prehnite is also present as reworked grains at the same site.

Basalt and Dolerite Clasts

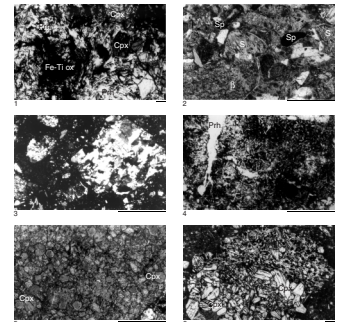
Clasts of mafic effusives and subintrusives occur at Site 1116 between 0.58 and 48.58 mbsf in Pliocene sandstones and conglomerates. Dolerites and basalts occur at Site 1108 between 245.19 and 437.82 mbsf in middle Pliocene sediments. In the northern margin at Site 1118, they occur in upper Miocene grainstones and sandstones and in the underlying conglomerates (between 861.18 and 878.69 mbsf). At Site 1115, they occur in upper Miocene conglomerates (between 566.83 and 566.89 mbsf), whereas at Site 1109 (between 763.66 and 765.79 mbsf), a dolerite basement is reworked as clasts in upper Miocene conglomerate.

Dolerite clasts show intersertal to rarer ophitic texture; basalts show a textural range from holocrystalline to hypocrySTALLINE with skeletal to spherulitic plagioclase. Olivine is present diffusely as phenocrysts or microphenocrysts (Pls. P2, fig. 2, P3, figs. 2, 4). Ilmenite is a diffuse accessory phase; in some clasts it exceeds 3% in volume, suggesting ferrobasalt compositions. The petrographic features of investigated clasts are consistent with tholeiitic magma series and are comparable with dolerites analyzed at Sites 1109, 1111, 1114, 1117, and 1118 that show enriched mid-ocean-ridge basalt similarities (Shipboard Scientific Party, 1999). On modal and textural grounds as a whole, the clasts represent the hypabyssal sheeted dikes (dolerite) and effusive parts of a tholeiitic sequence. The development of fast-cooling textures, comparable to those in pillow lavas, and evidence of spilitization are consistent with emplacement as submarine effusions.

Basalts and dolerites are pervasively altered; the albitization of plagioclase (\pm chlorite \pm calcite) and the replacement of olivine, glass, and, in part, pyroxene by phyllosilicates suggests spilitization as an alteration process. In Hole 1116A, prehnite veins cut dolerite clasts and plagioclase is altered to prehnite. More rarely, dolerite clasts are pervasively replaced by pumpellyite with minor prehnite. The marked green-yellow pleochroism of pumpellyite suggests Fe-rich composition.

The middle(?) Miocene conglomerates at Sites 1118 and 1109 include well-rounded dolerite and basalt clasts that show oxidative alteration produced in a tropical continental environment (Shipboard Scientific Party, 1999). Fragments with goethite concretions also support this hypothesis. The clasts reworked at Sites 1115 (middle Miocene packstones and sandstones) and 1116 (Pliocene sandstones and conglomerates) only in minor part show evidence of subaerial weathering, suggesting a provenance from deeper erosional levels.

P3. Photomicrographs of altered minerals, p. 43.



Alkalic Volcanic Clasts

In Hole 1115C (628.81 mbsf), alkalic volcanic clasts from middle Miocene fine-grained sandstone (Sample 180-1115C-37R-CC, 1.0–3.0 cm) are defined as tephrites; phenocrysts of zoned pyroxene with aegirine-augite rims, feldspathoid (sodalite/nosean), and rare biotite are present in feldspar microlith-rich glassy groundmass (Pl. P2, fig. 1). More rarely, phenocrysts of altered olivine constrain a basanite composition. This is the first recorded regional occurrence of alkaline volcanism of presumable early to middle Miocene age.

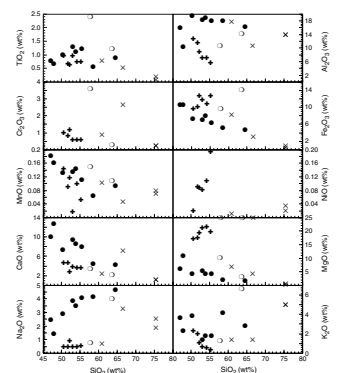
Calc-Alkaline Volcanic Clasts

Volcanics are present as (1) reworked lava fragments (up to 1 cm in size); (2) pumiceous clasts (up to 1 cm in size); (3) vitric shards; and (4) single-grain, more or less fragmented, phenocrysts (phenoclasts). The lava fragments are abundant, occurring in middle Pliocene to Pleistocene sediments in the footwall (Holes 1114A and 1116A) and rift basin (Site 1108). In the northern margin sequences, lava clasts are well represented since middle to late Miocene (Site 1115) and from early to middle Pliocene (Sites 1118 and 1109). Phenoclasts associated with shards and pumices, suggesting a significant explosive activity, are ubiquitous at all sites but are rare or lacking in the upper Pliocene sequence of the northern margin (Sites 1109, 1115, and 1118) (Tables T3, T4, T5).

The lava clasts show porphyric texture with glassy to microcrystalline groundmass, sometimes with fluidal texture. The mesostasis can be glassy to vitrophyric, rarely microcrystalline, with plagioclase microliths or sometimes alkali feldspar. Smith (1982), Smith and Milsom (1984), and Lackschewitz et al. (in press) evidenced the medium- to high-K character of the island-arc Miocene–Pliocene volcanism in the area. These volcanic types are mirrored by different phenocryst assemblages found in the glassy groundmass of basalt andesite composition (Fig. F3; Table T9); plagioclase + clinopyroxene ± orthopyroxene; plagioclase + red hornblende ± clinopyroxene, and, more rarely, plagioclase + red hornblende + biotite ± clinopyroxene. Plagioclase + clinopyroxene, plagioclase + biotite ± clinopyroxene, plagioclase + clinopyroxene + green hornblende ± biotite, and rarer quartz occur in a glassy groundmass of andesite to rhyolite composition. Sanidine sometimes included in biotite is rarely present among phenocrysts (Samples 180-1118A-66R-3, 24–28 cm, and 180-1108B-3R-1, 41–44.5 cm). The appearance or lack of hornblende (rarely biotite) in relatively primitive basalt andesite and andesite points to differing hydration conditions of the magmas. In spite of local prevalence of basalt andesite and andesite, a regular distribution over the sites and through time of the calc-alkaline terms is not recorded. However, quartz phenoclasts and quartz-bearing pumices are mostly present at the forearc sites.

The glassy groundmass of volcanic clasts from the northern margin, footwall, and rift sites was analyzed by electron microprobe. Many analyses have a low total oxide sum, likely due to incipient hydration processes and/or microvesicularity, and the compositional data are only approximate. Therefore, the reported analyses were selected (total oxide sum > 90 wt%) and recast to 100%. The glass shards range in composition from basalts to rhyolites (Fig. F3; Table T9) of calc-alkaline medium- and high-K series.

F3. Harker diagrams for glass fragments in volcaniclastic arenites, p. 18.



T9. Chemical composition of glass shards and volcanic clast groundmass, p. 36.

Trachyte clasts at Site 1116 represent the record of high-K to transitional (shoshonitic) volcanism in middle to upper Pliocene sandstones. Also at Sites 1110–1112, the talus sediments include acid-intermediate volcanics, quartz trachyte, and lamprophyre (Taylor et al., 1999). They have been related to intrusions within the Moresby Seamount and were eventually compared with the high-K volcanic equivalents of the Papuan Peninsula and D'Entrecasteaux Islands and to the Pliocene-Pleistocene comendites belonging to the Miocene Trobrian arc (Ashley and Flood, 1981).

Generally, the explosive products are present in epiclastic deposits from turbidity currents or mass flows and are associated with minor bioclastic and terrigenous materials. However, millimeter- to centimeter-thick layers composed of glass shards with pockets of phenoclasts and sparse pumices are relatively common mostly in the northern margin, interbedded with turbidites, and likely represent the deposition by fallout from onland eruptions (Samples 180-1109C-28X-1, 4–8 cm; 180-1109D-4R-7, 0–2 cm; 180-1115C-6R-2, 17–19 cm; and 180-1115C-10R-1, 5–7 cm). The explosive activity is mostly represented by felsic materials in accordance with the dacitic-rhyolitic nature of the glassy shards (Lackschewitz et al., in press) and by the presence of localized quartz phenoclasts, whereas quartz is rare in the lava clasts.

The volcanic clasts display moderate or no alteration at all. Alteration to phyllosilicate minerals (mostly celadonite) under low-temperature hydrothermal conditions can affect glass, biotite, and, more rarely, amphibole. Clasts in calcareous strata sometimes show partial syndiagenetic impregnation by carbonates. More rarely, andesite clasts affected by cortical carbonate replacement are subsequently rounded (Sample 180-1116A-16R-1, 103–107 cm).

Sedimentary Clasts

Sedimentary rock fragments are scant at all sites. In particular, silty claystone fragments were recovered in the rift basin in fine- to medium-grained sandstone (Sample 180-1108B-31R-2, 20.5–23.5 cm). In the footwall, siltstone fragments were recovered in the same lithology (Sample 180-1114A-14R-1, 106–108 cm) and limestone fragments in conglomerate (Sample 180-1116A-5R-1, 79–81 cm). In the same hole, limestone and siliceous sedimentary rock fragments are also present in conglomerate (Sample 180-1116A-6R-1, 37–39 cm).

A conglomerate sample (180-1116A-5R-1, 79–81 cm) contains a well-rounded chert clast with poorly preserved shells. The clast shows an evident oxidized rim, likely originating from prolonged subaerial exposition.

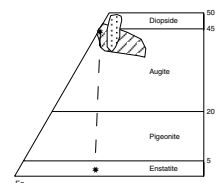
Mineral Chemistry

Pyroxenes

Clinopyroxenes in microgabbros vary in composition of clinopyroxenes from diopside with high wollastonite component to augite (Fig. F4).

In the calc-alkaline volcanics, clinopyroxene phenocrysts coexist with plagioclase (An_{50-43}) in basalt andesite to dacite glassy groundmass. Their compositions fall within the augite field, evolving from higher to lower Wo/En ratios in parallel with evolving glass composition. However, the complete evolution can be observed within the same zoned

F4. Composition of clinopyroxenes from volcanic and gabbroic rocks, p. 19.



grain. Coexisting clinopyroxene ($Wo_{37}En_{44}$) and orthopyroxene (En_{70}) were found in Sample 180-1114A-28R-CC, 3–5 cm. Representative analyses are reported in Table T10 and Figure F4.

Biotites

Analyzed biotites are optically homogeneous phenocrysts with constant composition; they are characterized by relatively high Mg content (Table T11) that points to phlogopite-rich compositions. The Al_{tot} -Mg correlation (Nachit et al., 1985) is consistent with pertinence to the calc-alkaline series.

Amphiboles

Igneous calcic amphiboles referable to the calc-alkaline volcanics were distinguished on the grounds of optical and compositional features (Table T12; Fig. F5): (1) red hornblende (high Al^{IV} - Al^{VI} ratios) present in the most primitive compositions (basalt andesites and andesites) and (2) green hornblendes (lower Al^{IV} - Al^{VI} ratios) that occur in relatively evolved andesites and dacites.

Colorless metamorphic hornblendes from chlorite-bearing schist show a low Al^{IV} - Al^{VI} ratio.

Feldspars

The composition of plagioclase in the gabbroic clasts varies between An 65 and 75 mol% (Table T13; Fig. F6). In calc-alkaline volcanic clasts, phenocrysts from basalt andesites have An_{42-55} mol%, whereas the corresponding microliths range between An 25 and 43 mol%. Anorthite <15 mol% is observed in the microliths of more felsic terms. Alkali feldspars with a wide Ab/Or compositional range were analyzed in high-K andesites; Or >90 mol% corresponds to K-feldspar in a rhyolite.

Spinel

Red spinel associated with serpentinite clasts shows homogeneous composition with $Mg = 67$ and $100 \times Cr/Cr+Al = 33$. Such composition is comparable to that observed in Cr-spinel of poorly depleted mantle lherzolites (Hoogerdujin Strating et al., 1990).

DISCUSSION

The set of data included in this chapter holds a meaning in a more comprehensive frame than that depicted at the regional scale by Robertson et al. (in press); however, the petrographic detail on lithic fragments allows significant considerations.

Serpentinites and tholeiitic basalts, dolerites, and gabbros are ascribed to the Paleogene Papuan ophiolite belt (Taylor et al., 1999; Robertson et al., in press). Moreover, dolerites represent the drilled basement of the northern margin (Site 1109) and footwall (Site 1114) of the Moresby Seamount. Gabbros, at places foliated, are present at Site 1117 (Shipboard Scientific Party, 1999).

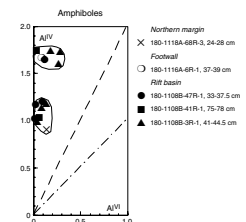
In the different environments of the basin, ophiolitic clasts show a dishomogeneous distribution; in the northern margin (Sites 1109, 1115, and 1118), basalts, dolerites, and gabbros are the main constitu-

T10. Analyses of clinopyroxene phenocrysts, p. 37.

T11. Analyses of biotite phenocrysts, p. 38.

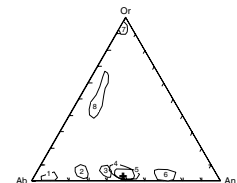
T12. Analyses of amphibole phenocrysts and phenocrasts, p. 39.

F5. Al^{IV} - Al^{VI} correlation for calcic amphiboles, p. 20.



T13. Analyses of plagioclase microliths, phenocrysts, and phenocrasts, p. 40.

F6. Plagioclase compositions measured in volcanic and intrusive rocks from drilled sites, p. 21.



ents in conglomerates and are present in sandstones and limestones since middle to late Miocene, but are lacking in the Pliocene sediments. Serpentinite clasts were exceptionally recovered only in an upper Miocene carbonatic level (Site 1115). At the footwall, basalts, dolerites, gabbros, and serpentinites are relatively common in the Pliocene sediments at Site 1116, but lacking at Site 1114. This suggests that already since Pliocene the two sites had a different position relative to the ophiolitic source.

In the rift basin (Site 1108), basalts and gabbros appear associated with metamorphic rocks in the lower levels of middle Pliocene age, whereas serpentinites are diffuse since Pliocene to Pleistocene times.

All over the basin, basalts, dolerite, and gabbro clasts commonly exceed 3–10 mm in size; serpentinite clasts are present as fine- to medium-grained sands. Moreover in the northern margin, the tholeiitic clasts show frequent weathering that constrains a prolonged exposure under subaerial conditions. Such evidence is uncommon in the clasts from the footwall and the rift basin, and rare oxidized serpentinite clasts were observed. On the whole, it is likely to envisage that at the northern margin sites felsic clasts experienced relatively short-range transport and originate from sources internal to the basin as a consequence of erosion of the ophiolitic basement. The footwall and rift basin ophiolitic clasts are present in relatively proximal turbidites associated with metamorphic rocks and granites. Conversely, a transport from farther sources can be envisaged at least for part of the serpentinite clasts.

The prevalence of basalt and dolerite clasts and the evolved composition of most gabbros likely originated from uppermost levels of oceanic layer 3, in accordance with erosion restricted to shallow portions of the ophiolitic basement. The greenschist facies alteration of some gabbroic clasts associated with schistosity is not in contrast and can be correlated with early tectonic events developed under high thermal gradient conditions during the build up of the ophiolite sequence, also consistent with shear textures at Site 1117. On the other hand, restricted to Site 1116, rare clasts affected by prehnite-pumpellyite facies overprint support pressures of ~0.2–0.3 GPa (Bucher and Frey, 1994). This requires that portions of the ophiolitic basement attained a lithostatic load of some (≥ 5) kilometers, for instance, in an incipient intra-oceanic subduction prior to uplift and erosion. On the whole, the petrographic features and stratigraphic position of the ophiolite clasts at the northern margin sites are evidence of origins by reworking of subaerial deposits during the early Miocene phases of basin development. In contrast, the ophiolite clasts from the footwall and rift basin suggest that portions of the ophiolitic basement, eventually affected by older tectonics, were uplifted by extensional phases already active since the Pliocene in adjacent areas.

This hypothesis can also account for the presence and distribution of metamorphic rocks and granite clasts. Metamorphic rocks could either (1) represent continental lithosphere associated with granites, (2) represent equivalents of the metamorphosed accretionary complex underlying the Papuan ophiolitic thrust (Davies, 1980a), or (3) be assimilated with the metasediments outcropping at the D'Entrecasteaux Islands (Davies, 1980b; 1990). The significance of metamorphic rocks as substrate unroofed together with the overlying ophiolites is likely and consistent with data from Sites 1111 and 1113 (Taylor et al., 1999). Talc schists, chlorite schists, serpentine schists, and epidiosites interpreted as

fault gauge clasts can be considered as the evidence for exhumation of ophiolitic and metamorphic materials along tectonic discontinuities.

Tephrite and basanite clasts (middle Miocene sediments in the northern margin, Site 1115) are significant, although localized. The clasts (a few millimeters to 1 cm in size) are poorly rounded and show unaltered glassy groundmass and therefore did not undergo the weathering processes affecting the ophiolitic clasts from the same stratigraphic levels. An early to middle Miocene age and moderate transport can therefore be envisaged. The clasts constrain an alkaline volcanism that cannot be compared with the middle Pliocene–Holocene shoshonitic volcanism including the trachyte clasts (Site 1116) also reported from Sites 1110–1113 (Taylor et al., 1999) and well represented in the area (Smith et al., 1977; Smith and Milsom, 1984; Stolz et al., 1993; Ashley and Flood, 1981). More unlikely, the shoshonitic volcanism, generally subduction-related volcanic sequences including basanites and tephrites, are reported from a continental rift environment (Wilson, 1991).

The remarkable compositional range of arc-related volcanic products including basalt andesites to rhyolites and medium- to high-K calc-alkaline to rare shoshonite compositions is consistent with the provenance of fragments from several volcanic centers and with a temporal evolution of the volcanism, although a space and time volcanic zoneography has not been evidenced.

Clasts reworked in the turbidity currents include a wide range of textural features from porphyritic lavas, glassy to microcrystalline variably vesicular groundmass, pumices, glass shards, and single-grain phenocrysts. Rarer millimeter-sized clasts with granophyric texture could result from the blast of subvolcanic felsic bodies. Mostly in northern margin sites through the lower to middle Pliocene, the occurrence of tephra layers interbedded with turbidite evidences episodic contribution from air fall ashes.

CONCLUSIONS

On the whole, the analyzed lithic fragments provide a set of data that largely fits the two-stage model depicted for the evolution of the Woodlark Basin between the late Miocene–Pliocene and Pliocene–Holocene summarized by Robertson et al. (in press) on the grounds of onland geology, geophysical, and drill evidence. The petrographic detail of the nature and distribution of the lithic clasts and grains allows some constraints of the major tectonic and volcanic events.

The clast assemblages at the footwall sites evidence (1) the nature of the oceanic slice exhumed, including generally evolved basaltic effusives and intrusives; (2) the ultramafic rocks that likely pertain to the same ophiolitic complex are restricted to transport by turbidity currents and likely derive from onland outcrops; and (3) the origin of some lithologies by uplift from relatively deep levels, implying extensional tectonics active at least since the middle Pliocene.

Calc-alkaline volcanism is recorded in the sedimentary sequences in continuity with the arc-related products from the Papuan Peninsula and D'Entrecasteaux Islands and to the latest volcanics of the Miocene Trobrian arc. The arc volcanism shows a wide compositional range from medium- to high-K and shoshonitic products; however, no apparent temporal evolution arises from the stratigraphic setting. Lava clasts, volcanogenic grains, and glass shards derive from transport by turbidity currents, whereas in the northern margin Pliocene, the increasing fre-

quency of tephra mostly composed of glass shards and vesicular silicic fragments suggests a transition to more explosive activity and contribution to the sediments from aerial fallout materials.

Evidence of localized alkalic volcanism of presumable early to middle Miocene age is a new finding. It could represent a rift phase earlier than or coeval to the first opening of the Woodlark Basin or, less probably, could derive by depositional trajectories diverted from an adjacent basin.

ACKNOWLEDGMENTS

This research used samples and/or data provided by the Ocean Drilling Program (ODP). ODP is sponsored by the U.S. National Science Foundation (NSF) and participating countries under management of Joint Oceanographic Institutions (JOI), Inc. Funding for this research was provided by CNR funds to I. Premoli (University of Milano) and to E. Andri and L. Cortesogno (University of Genova). The authors wish to thank L. Negretti for help in mineral data acquisition, T. Cucchiara for XRD analyses, and R. Rubiera for calcimetries.

REFERENCES

- Ashley, P.M., and Flood, R.H., 1981. Low-K tholeiites and high-K igneous rocks from Woodlark Island, Papua New Guinea. *J. Geol. Soc. Aust.*, 28:227–240.
- Bouma, A.H., 1962. *Sedimentology of Some Flysch Deposits: A Graphic Approach to Facies Interpretation*: Amsterdam (Elsevier).
- Bucher, K., and Frey, M., 1994. *Petrogenesis of Metamorphic Rocks*: Berlin (Springer-Verlag).
- Davies, H.L., 1980a. Crustal structure and emplacement of ophiolite in southeastern Papua New Guinea. *Colloques Internationaux du C.N.R.S.*, 272:17–33.
- , 1980b. Folded thrust fault and associated metamorphics in the Suckling-Dayman Massif, Papua New Guinea. *Am. J. Sci.*, 280-A:171–191.
- , 1990. Structure and evolution of the border region of New Guinea. In Carman, G.J., and Carman, Z. (Eds.), *Petroleum Exploration in Papua New Guinea: Proc. 1st PNG Petrol. Conv.*: Port Moresby, Papua New Guinea (PNG Chamber of Mines and Petroleum), 245–250.
- Goodliffe, A.M., 1998. The rifting of continental and oceanic lithosphere: observations from the Woodlark Basin [Ph.D. thesis]. Univ. Hawaii, Honolulu.
- Goodliffe, A.M., Taylor, B., Martinez, F., Hey, R.N., Maeda, K., and Ohno, K., 1997. Synchronous reorientation of the Woodlark Basin spreading center. *Earth Planet. Sci. Lett.*, 146:233–242.
- Hedges, J.I., and Stern, J.H., 1984. Carbon and nitrogen determinations of carbonate-containing solids. *Limnol. Oceanogr.*, 29:657–663.
- Hoogerduijn Strating, E.H., Piccardo, G.B., Rampone, E., Scambelluri, M., and Vissers, R.L.M., 1990. The structure and petrology of the Erro-Tobbio peridotite, Voltri Massif, Ligurian Alps: guidebook for a two-day excursion with emphasis on processes in the upper mantle (Voltri Massif, June 26–28, 1989). *Ophioliti*, 15:119–184.
- Lackschewitz, K., Bogaard, P.V.D., and Mertz, D.F., in press. $^{40}\text{Ar}/^{39}\text{Ar}$ ages of fallout tephra layers and volcanoclastic deposits in the sedimentary succession of the western Woodlark Basin, Papua New Guinea: the marine record of Miocene–Pleistocene volcanism. In Wilson, R.C.L., Beslier M.-O., Whitmarsh, R.B., Froitzheim, N., and Taylor, B. (Eds.), *Non-volcanic Rifting of Continental Margins: A Comparison of Evidence from Land and Sea*, Spec. Publ.—Geol. Soc. London. [N1]
- Morimoto, N., Fabries, J., Ferguson, A., Ginzburg, I., Roos, M., Seifert, F., and Zussman, J., 1988. Nomenclature of pyroxenes. *Bull. Mineral.*, 111:535–550.
- Nachit, H., Razafimahefa, N., Stussi, J.-M., and Carron, J.-P., 1985. Composition chimique des biotites et typologie magmatique des granitoides. *C.R. Seances Acad. Sci. Ser. 2*, 301:813–818.
- Robertson, A.H.F., Awadallah, S.A.M., Gerbaudo, S., Lackschewitz, K.S., Monteleone, B.D., Sharp, T.R., and Leg 180 Shipboard Party, in press. Sedimentary-tectonic evolution of the Miocene–Recent Woodlark basin, SW Pacific: implications for rift processes. *Spec. Publ.—Geol. Soc. London*. [N2]
- Rock, N.M.S., 1990. The International Mineralogical Association (IMA/CNMMN) pyroxene nomenclature scheme: computerization and its consequences. *Mineral. Petrol.*, 43:99–119.
- Rock, N.M.S., and Leake, B.E., 1984. The International Mineralogical Association amphibole nomenclature scheme: computerization and its consequences. *Mineral. Mag.*, 48:211–227.
- Shipboard Scientific Party, 1999. Leg 180 Summary: Active Continental Extension in the Western Woodlark Basin, Papua New Guinea. In Taylor, B., Huchon, P., Klaus, A., et al. *Proc. ODP, Init. Repts.*, 180, 1–77 [CD-ROM]. Available from: Ocean Drilling Program, Texas A&M University, College Station, TX 77845-9547, U.S.A.
- Smith, I.E.M., 1982. Volcanic evolution in eastern Papua. *Tectonophysics*, 87:315–333.

- Smith, I.E.M., Chappell, B.W., Ward, G.K., and Freeman, R.S., 1977. Peralkaline rhyolites associated with andesitic arcs of the southwest Pacific. *Earth Planet. Sci. Lett.*, 37:230–236.
- Smith, I.E.M., and Milsom, J.S., 1984. Late Cenozoic volcanism and extension in eastern Papua. In Kokelaar, B.P., and Howells, M.F. (Eds.), *Marginal Basin Geology*. Spec. Publ.—Geol. Soc. London, 16:163–171.
- Stolz, A.J., Davies, G.R., Crawford, A.J., and Smith, I.E.M., 1993. Sr, Nd and Pb isotopic compositions of calc-alkaline and peralkaline silicic volcanics from the D'Entrecasteaux Islands, Papua New Guinea, and their tectonic significance. *Mineral. Petrol.*, 47:103–126.
- Taylor, B., Goodliffe, A., Martinez, F., and Hey, R., 1995. Continental rifting and initial sea-floor spreading in the Woodlark Basin. *Nature*, 374:534–537.
- Taylor, B., Goodliffe, A.M., and Martinez, F., 1999. How continents break up: insights from Papua New Guinea. *J. Geophys. Res.*, 104:7497–7512.
- Weissel, J.K., Taylor, B., and Karner, G.D., 1982. The opening of the Woodlark basin, subduction of the Woodlark spreading system, and the evolution of northern Melanesia since mid-Pliocene time. *Tectonophysics*, 87:253–277.
- Wilson, M., 1991. *Igneous Petrogenesis*: London (Harper Collins Academic).

Figure F1. A. Major physiographic features and active plate boundaries of the Woodlark Basin region. The stippled area encloses oceanic crust formed during the Brunhes Chron at spreading rates labeled in millimeters per year. MT = Moresby transform fault, ST = Simbo transform fault, DE = D'Entrecasteaux Islands. Inset = the geographic location of the Woodlark Basin. B. Nested meridional sections at 151°34.5'E showing the regional bathymetry. C. Local structures across the incipient conjugate margins. Leg 180 drill sites are depicted on the B sections. VE = vertical exaggeration. From Shipboard Scientific Party, 1999.

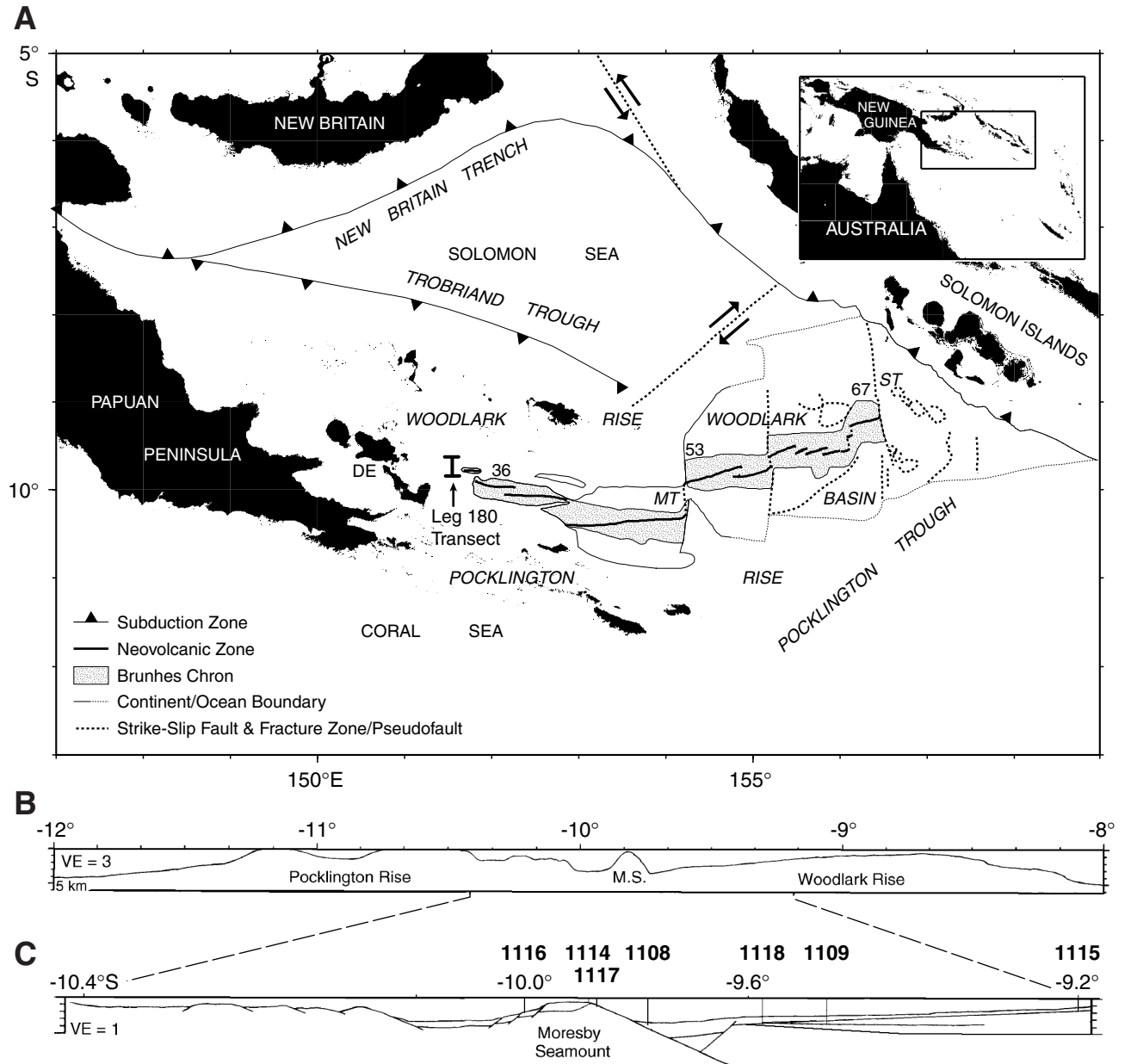


Figure F2. CaCO₃ downhole in (A) rift Site 1108, northern margin Sites (B) 1118, (C) 1109, (D) 1115, and footwall Sites (E) 1116 and (F) 1114.

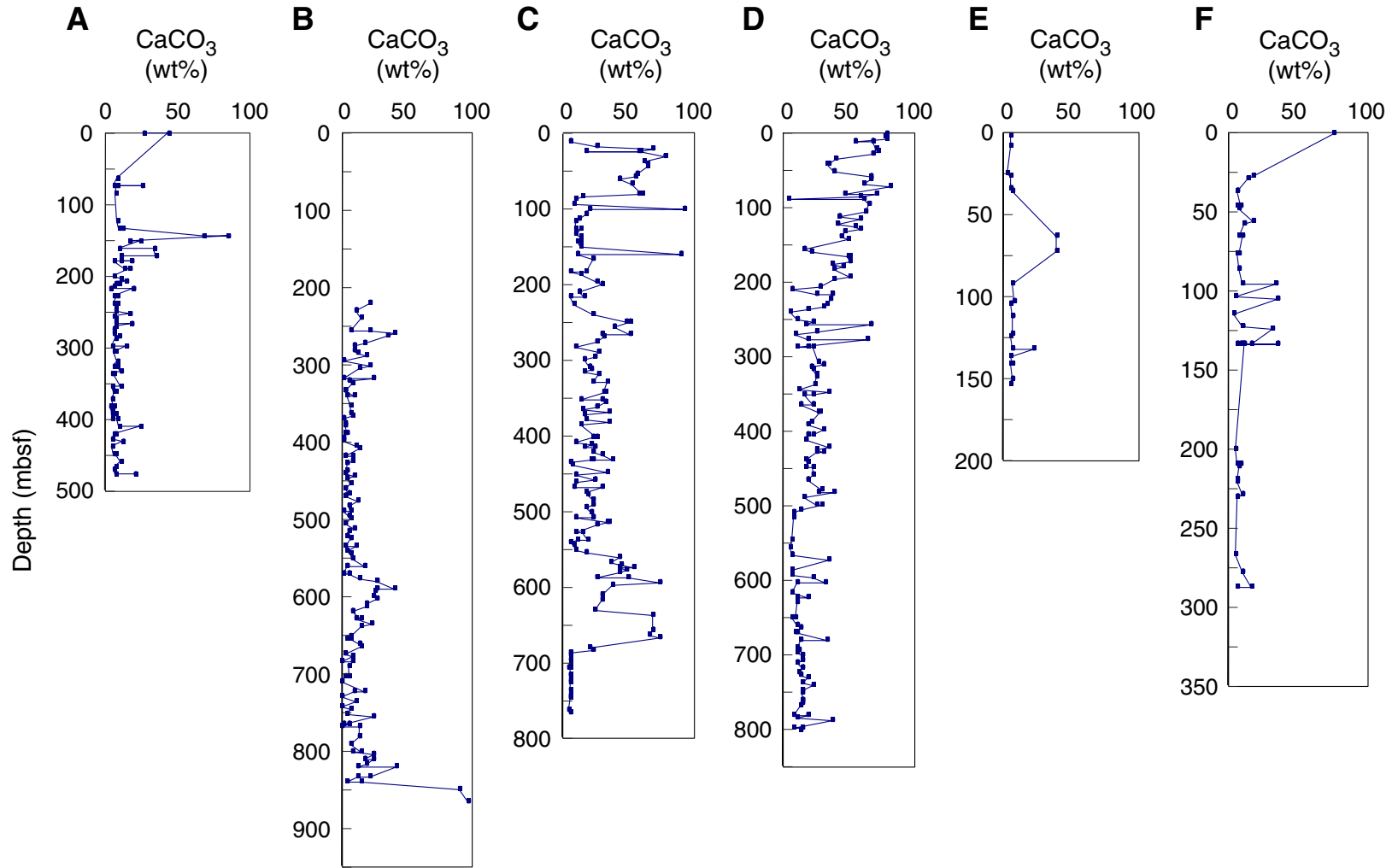


Figure F3. Harker diagrams for glass fragments in volcaniclastic arenites. Circles = northern margin sites, crosses = rift basin sites, oblique crosses = footwall sites, solid circles = data from late Cenozoic arc trench-type volcanism in southeastern Papua, from Smith (1982).

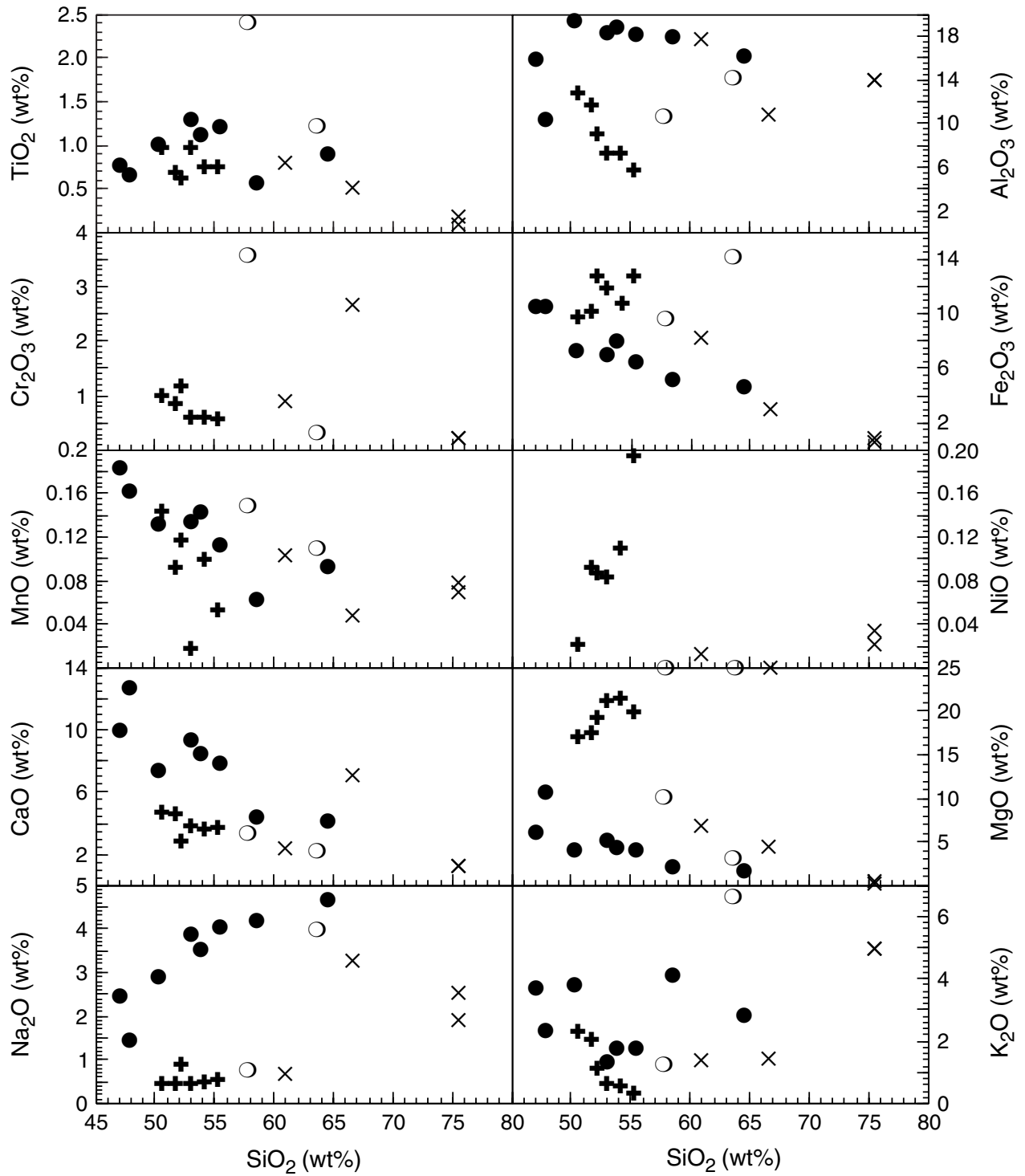


Figure F4. Composition of clinopyroxenes from volcanic (field with diagonal lines) and gabbroic (field with squares) rocks.

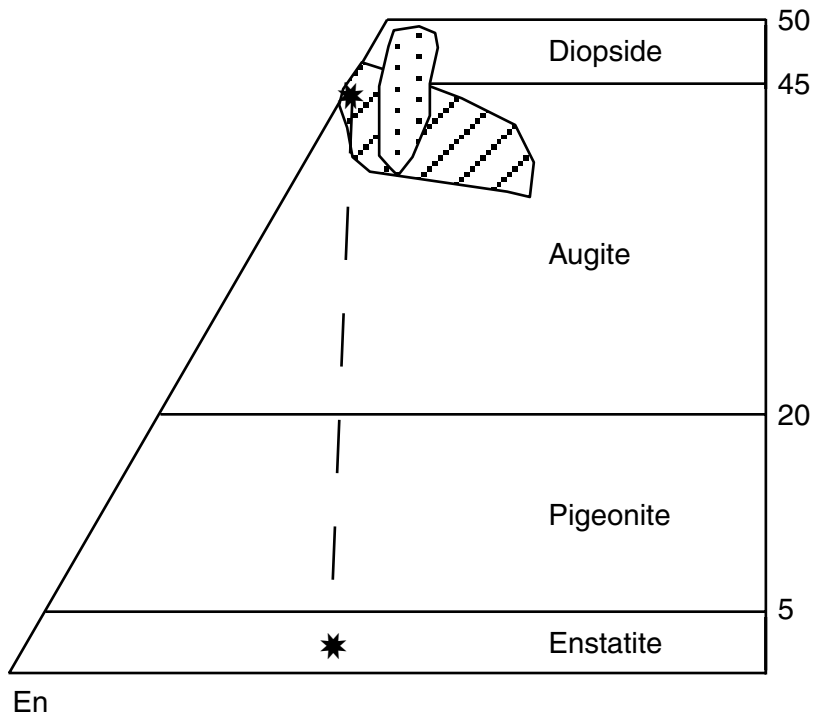


Figure F5. Al^{IV}-Al^{VI} correlation for calcic amphiboles. Oblique cross = amphibole from Chl-Am schist. High Al^{IV} field = red hornblende phenocrysts from basalt andesites and andesites. Low Al^{IV} field = green hornblende phenocrysts in andesites and dacites.

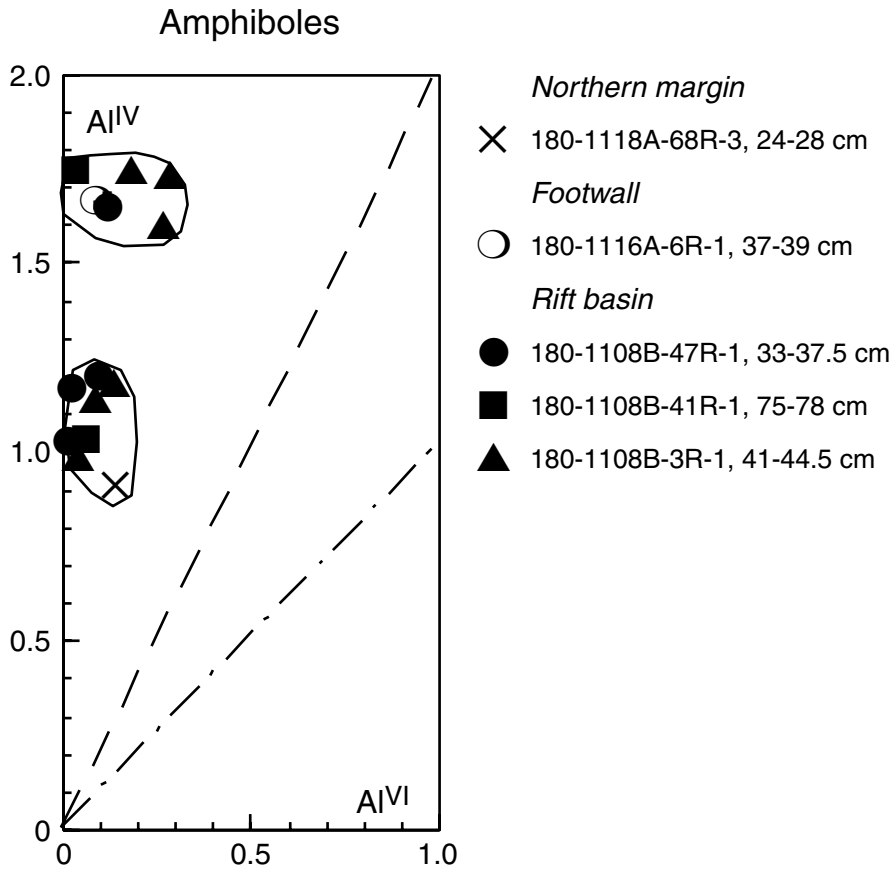


Figure F6. Plagioclase compositions measured in volcanic and intrusive rocks from drilled sites. 1 = microliths from rhyolitic glass, 2 = microliths in andesite, 3 = microliths in basaltic andesite, 4 = phenocrysts in andesite, 5 = phenocrysts in basalt and basaltic andesite, cross = phenocrysts in high-K andesite, 6 = microgabbro, 7 = K-feldspar in rhyolitic glass, 8 = alkali-feldspars in high-K andesite, Or = orthoclase, Ab = albite, An = anorthite.

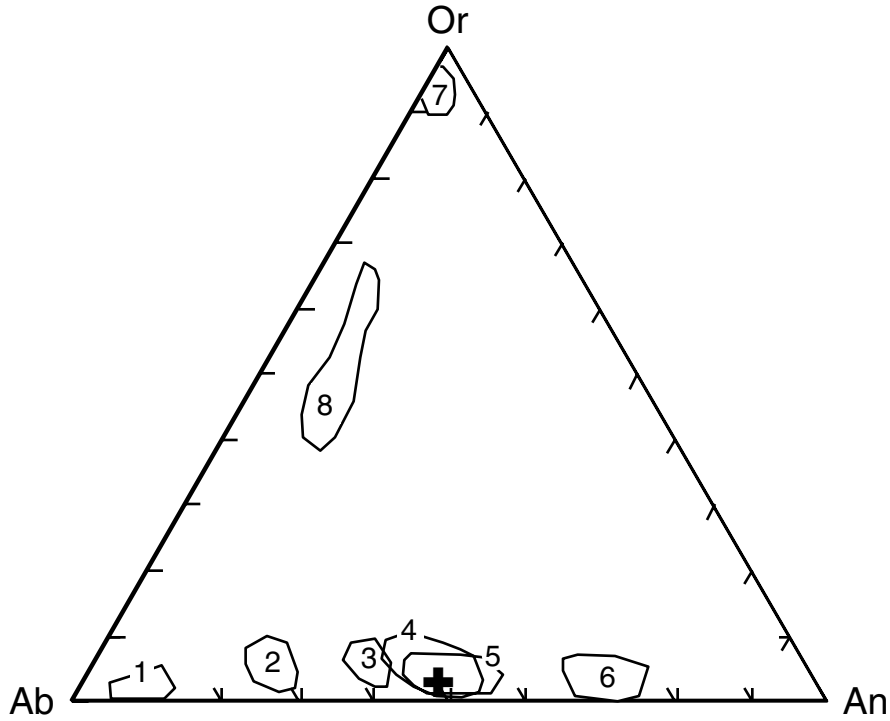


Table T1. Petrographic features of sediments from footwall Sites 1114 and 1116. (See table notes. Continued on next page.)

Age	Core, section, interval (cm)	Depth (mbsf)	Lithology	Matrix/Cement	Lithic fragments	Bioclasts	Organic carbon
Quaternary? middle to late Pliocene	180-1114A- 1R-CC, 1–6	0.01	Nannofossil-foraminifer sand				
	1R-CC, 34–36	0.34	Siltstone	Carbonatic, argillaceous	Volcanics	Planktonic and benthic foraminifers	
	3R-1, 50–52	17.10	Fine-grained sandstone	Carbonatic, argillaceous, volcanic	Shards	Foraminifers, shell debris	X
	5R-1, 24–26	36.04	Fine-grained sandstone	Carbonatic, argillaceous, volcanic	Shards	Foraminifers, shell debris	X, as ribbons
	6R-2, 68–72	46.65	Silty clay	Argillaceous	Shards		
	8R-1, 16–20	64.76	Siltstone	Argillaceous	Altered shards, volcanics	Shell debris	
	9R-2, 15–17	75.77	Fine-grained sandstone	Argillaceous		Foraminifers, shell debris	X
	11R-CC, 18–20	95.24	Fine-grained sandstone	Carbonatic matrix		Foraminifers	X
	12R-1, 3–4	103.23	Fine-grained sandstone	Carbonatic matrix			
	12R-1, 88–91	104.08	Carbonaceous fine-grained sandstone	Carbonatic matrix	Shards, volcanics	Shell debris	
	13R-1, 90–93	113.70	Fine- to medium-grained sandstone	Glassy	Shards, volcanics		
	14R-1, 96–98	123.36	Siltstone	Argillaceous, glassy		Foraminifers, shell debris	X
	14R-1, 106–108	123.46	Fine- to medium-grained sandstone		Andesites, siltstones	Benthic foraminifers	
	15R-1, 46–48	132.46	Fine- to coarse-grained sandstone	Carbonatic cement	Andesites		
	16R-CC, 12–15	141.72	Medium-grained sandstone		Andesites		
	21R-1, 11–14	189.91	Fine-grained sandstone		Andesites		
	22R-1, 74–76	200.14	Fine-grained sandstone	Carbonatic, argillaceous, glassy	Shards	Shell debris	X
	22R-1, 77–80	200.17	Sandy siltstone	Argillaceous	Volcanics, serpentine schists, chlorite schists	Planktonic foraminifers	X
	23R-1, 70–72	209.50	Fine-grained sandstone	Carbonatic, argillaceous, glassy	Shards	Shell debris	X
	24R-1, 33–35	218.72	Coarse-grained sandstone		Andesites, felsites		
	24R-2, 20–23	218.99	Coarse-grained sandstone				
	26R-1, 96–97	238.56	Coarse-grained sandstone	Glassy	Shards, andesites, felsites		
	26R-CC, 1–3	238.82	Coarse-grained sandstone				
	27R-CC, 9–21	247.49	Coarse-grained sandstone				
	28R-CC, 3–5	256.93	Coarse-grained sandstone		Granite		
	28R-CC, 3–7	256.93	Coarse-grained sandstone	Argillaceous	Andesites, felsites, chlorite schists		
	30R-1, 47–51	276.57	Silty claystone	Argillaceous			
	30R-CC, 1–4	277.07	Fine- to medium-grained sandstone	Glassy	Shards, volcanics		
	31R-1, 15–17	285.95	Calcareous silty clay	Argillaceous			
	Pliocene	180-1116A- 1R-1, 58–60	0.58	Medium- to coarse-grained sandstone	Glassy	Shards, felsites, andesites, trachytes, basalts, gabbros, serpentinites, granites, amphibole schists, talc schists	Shell debris
2R-CC, 11–14		8.0	Sandy siltstone				
3R-1, 13–15		16.33	Fine-grained sandstone	Carbonatic matrix	Volcanics, basalts, serpentinites, chlorite schists	Shell debris	X, as ribbons
3R-1, 42–44		16.62					
4R-2, 1–4		25.51	Silty sandstone				
5R-1, 18–20		33.98					
5R-1, 79–81		34.59	Orthoconglomerate	Argillaceous	Andesites, basalts, dolerites, gabbros, limestones		
6R-1, 9–11		42.49	Conglomerate	Carbonatic matrix	Andesites, dolerites, gabbros, serpentinites, Prh-Pmp metabasalts	Benthic foraminifers, algae	
6R-1, 37–39		42.77	Conglomerate	Carbonatic matrix	Andesites, dolerites, gabbros, serpentinites, Prh-Pmp metabasalts		

Table T1 (continued).

Age	Core, section, interval (cm)	Depth (mbsf)	Lithology	Matrix/Cement	Lithic fragments	Bioclasts	Organic carbon
	7R-1, 58–60	48.58	Conglomerate	Carbonatic matrix	Andesites, trachytes, basalts, dolerites, gabbros, cherts		
	7R-CC, 5–7	48.67	Silty sandstone	Argillaceous	Andesites		
	9R-1, 122.5–126	63.83	Silty sandstone	Carbonatic cement		Foraminifers	
	9R-1, 138–141	63.98	Carbonaceous fine-grained sandstone	Carbonatic matrix			
	11R-1, 16–19	81.96	Medium-grained sandstone	Argillaceous	Volcanics	Shell debris	
	12R-1, 2–6	91.42	Fine-grained sandstone	Argillaceous	Volcanics, serpentine schists, prehnite		
	13R-2, 25–27	102.07	Fine-grained sandstone	Glassy	Shards	Shell debris	
	13R-4, 51–54	103.55	Fine-grained sandstone	Glassy	Shards	Shell debris	
	14R-1, 50–52	111.10	Fine- to medium-grained sandstone	Argillaceous			
	16R-1, 103–106	131.03					
	16R-1, 103–107	131.03	Fine- to medium-grained sandstone	Argillaceous	Andesites	Foraminifers	
	16R-3, 6–8	132.22					
	16R-3, 134–136	133.50	Fine-grained sandstone	Glassy, argillaceous	Shards, volcanics	Benthic and planktonic foraminifers	X
	17R-2, 53–55	141.73	Interbedded fine-grained sandstone and siltstone	Cement/argillaceous	Volcanics	Benthic foraminifers	
	18R-1, 30–32	149.60	Interbedded fine-grained sandstone and siltstone	Cement/argillaceous	Volcanics	Benthic foraminifers	
	18R-2, 11–15	150.32	Interbedded medium-grained sandstone and siltstone	Cement/argillaceous	Volcanics	Benthic foraminifers	

Notes: Lithic fragments: gabbro includes olivine gabbro, oxide gabbro, and diorite compositions; basalt and dolerite refer to tholeiitic serial affinity; andesite includes calc-alkaline basalt andesite and andesite to quartz andesite; felsite refers to dacite and rhyolite compositions; trachyte includes lava clasts and glass with K-feldspar microliths; granophyre indicates fine-grained eutectic quartz-feldspar intergrowth; shards include ash fall tephra or prevalent glassy matrix in turbidites; volcanics include fragments of uncertain definition. Prh = prehnite, Pmp = pumpellyite, X = present.

Table T2. Petrographic features of sediments from rift basin Sites 1108, 1110, 1111, and 1112. (See table notes. Continued on next page.)

Age	Core, section, interval (cm)	Depth (mbsf)	Lithology	Matrix/Cement	Lithic fragments	Bioclasts	Organic carbon
Pleistocene	180-1108B-1R-2, 57-63	1.57	Clay-bearing nannofossil ooze				
	3R-CC, 0-4	14.50	Medium- to coarse-grained sandstone	Carbonatic cement	Shards, andesites, felsites, serpentinites, granites, serpentine schists, talc schists, chlorite schists	Foraminifers, bryozoans	
	3R-CC, 16-20	14.66	Sandy siltstone	Cement	Shards, andesites, serpentinites, serpentine schists, talc schists		
middle Pliocene	5R-CC, 6-8	33.86	Fine-grained sandstone	Carbonatic cement	Shards, andesites, serpentinites, talc schists		
	10R-1, 84-86	82.74	Mixed lithic sand				
	14R-2, 2-4	121.38	Fine-grained sandstone	Argillaceous matrix	Volcanics	Foraminifers	
	15R-1, 11-14	129.91	Fine-grained sandstone	Carbonatic cement	Shards, andesites, talc schists	Bryozoans and benthic foraminifers	
	16R-CC, 1-2	142.05	Packstone			Planktonic foraminifers	
	16R-CC, 4-6	142.08	Calcareous sandstone				
	19R-3, 6-9	169.86	Foraminifer-rich clayey siltstone				
	20R-CC, 0-3	180.55	Medium-grained sandstone	Matrix	Shards, andesites, felsites, serpentinites, amphibole schists	Bryozoans and benthic foraminifers	
	21R-CC, 1-3	189.08	Silty claystone		Andesites	Planktonic and benthic foraminifers	
	22R-4, 61-64	202.31	Normal graded fine-grained sandstone	Argillaceous/glassy matrix	Shards, andesites	Planktonic and benthic foraminifers, ostracodes	
	22R-6, 21-22	204.87	Fine-grained sandstone	Carbonatic cement	Andesites		
	23R-3, 34-36	210.15	Medium-grained sandstone	Argillaceous matrix	Andesites	Benthic foraminifers	
	25R-1, 78.5-81.5	226.79	Interbedded fine-grained sandstone and siltstone	Cement/matrix	Shards, chlorite schists	Benthic and planktonic foraminifers, bryozoans	
	26R-3, 17-21	238.77	Fine-grained sandstone		Serpentinites		
	26R-3, 39-41	238.99	Fine-grained sandstone		Serpentinites		
	27R-1, 29-33	245.19	Medium-grained sandstone		Andesites, basalts, dolerites, serpentinites (oxidized), granites, talc schists, amphibolites		
	27R-5, 60-62	251.51	Coarse-grained sandstone	Matrix	Andesites, felsites, basalts, volcanics, granites, gneissic rocks, epidiosites, foliated metabasites		
	27R-5, 66-70	251.56	Sandstone				
	28R-3, 28-31	257.46	Fine-grained sandstone	Glassy matrix	Shards, volcanics	Shell debris, ostracodes	
	28R-4, 68-70	258.77	Sandstone				
29R-1, 54-58	264.64	Sandstone					
30R-3, 44-46	276.39	Medium-grained sandstone		Andesites, talc schists	Shell debris		
31R-2, 20.5-23.5	284.68	Fine- to medium-grained sandstone	Cement/argillaceous matrix	Shards, talc schists, silty claystones	Benthic foraminifers, red algae, shell debris		
32R-3, 61-64	295.67	Medium-grained sandstone	Cement/argillaceous matrix	Andesites			
33R-1, 41-44.5	302.71	Medium-grained sandstone		Andesites, serpentinites, amphibole schists, quartz schists, chlorite schists, talc schists			
34R-2, 126-128	314.60	Coarse-grained sandstone		Shards, andesites, felsites			
36R-1, 82-86	332.12	Fine- to medium-grained sandstone with granules and pebbles		Andesites, basalts, talc schists, limestones			
36R-3, 0-4	333.42	Medium-grained sandstone		Andesites, serpentinites, talc schists			
36R-3, 52-56	333.94	Medium-grained sandstone		Andesites, serpentinites, talc schists	Shell debris		
37R-1, 13-16	341.03	Medium-grained sandstone		Andesites, basalts			
37R-4, 8-11	344.87	Fine- to coarse-grained sandstone		Andesites, basalts			
39R-1, 94-96	361.02	Fine-grained sandstone		Quartz-arenites	Planktonic foraminifers		

Table T2 (continued).

Age	Core, section, interval (cm)	Depth (mbsf)	Lithology	Matrix/Cement	Lithic fragments	Bioclasts	Organic carbon
	41R-1, 64–68	380.04	Medium-grained sandstone		Andesites		
	41R-1, 75–78	380.15	Fine-grained sandstone	Glassy matrix	Shards, andesites	Foraminifers	
	44R-1, 128–131	409.48	Calcareous sandy siltstone	Carbonatic/argillaceous matrix			
	45R-CC, 8–10	419.64	Fine-grained sandstone	Argillaceous matrix		Benthic foraminifers, shell debris	
	47R-1, 33–37.5	437.43	Fine-grained sandstone		Andesites, basalts, dolerites, gabbros, granites	Shell debris	
	47R-CC, 5–7	437.82	Conglomerate	Argillaceous matrix	Altered shards, andesites, dolerites, metabasites		
	47R-CC, 25–29	438.01	Medium-grained sandstone	Carbonatic cement, argillaceous matrix	Altered shards, volcanics		
	48R-2, 86–89	448.16	Fine-grained sandstone	Cement, argillaceous matrix	Volcanics		X, as ribbons
	49R-CC, 5–6	456.87	Medium-grained sandstone		Shards, volcanics		
Quaternary	180-1110A-1H-3, 52–54	3.52	Calcareous silty claystone				
Pleistocene	180-1111A-8R-2, 77–81	68.47	Silty clay				
	13R-2, 89–93	118.05	Calcareous clayey silt				
Pleistocene	180-1112A-1R-2, 20–23	1.70	Calcareous silty clay				X
	3R-1, 2–5	20.52	Silty sandstone	Matrix	Shards		X, as ribbons
	6R-1, 10–12	49.40	Fine-grained sandstone				
	9R-CC, 25–27	78.15	Medium-grained sandstone	Matrix	Andesites, felsites, basalts, volcanics, granites, gneissic rocks, epidiosites, foliated metabasites		

Notes: Lithic fragments: gabbro includes olivine gabbro, oxide gabbro, and diorite compositions; basalt and dolerite refer to tholeiitic serial affinity; andesite includes calc-alkaline basalt andesite and andesite to quartz andesite; felsite refers to dacite and rhyolite compositions; trachyte includes lava clasts and glass with K-feldspar microliths; granophyre indicates fine-grained eutectic quartz-feldspar intergrowth; shards include ash fall tephra or prevalent glassy matrix in turbidites; volcanics include fragments of uncertain definition. Prh = prehnite, Pmp = pumpellyite, X = present.

Table T3. Petrographic features of sediments from Woodlark Basin northern margin Site 1109. (See table notes. Continued on next page.)

Age	Core, section, interval (cm)	Depth (mbsf)	Lithology	Matrix/Cement	Lithic fragments	Bioclasts	Organic carbon
	180-1109C-						
Pleistocene	2H-4, 17-20	12.07	Clay				
	4H-5, 81-83.5	33.21	Calcareous clayey silt				
	4H-5, 85.5-88.5	33.26	Calcareous silty clay				
middle to late Pliocene	5H-2, 115-117	38.55	Calcareous clayey siltstone				
	5H-5, 29-31	42.19	Calcareous clay				
	7H-3, 23-25	58.13	Calcareous clayey silt				
	9H-6, 11.5-17.5	81.51	Calcareous clayey silt				
	11H-7, 36-39	101.76	Foraminifer-rich sand				
	12X-4, 115-118	108.05	Calcareous silty clay				
	18X-1, 67-69	160.77	Calcareous sandy silt				
	21X-CC, 40, 42	189.28	Packstone	Argillaceous		Benthic foraminifers, mollusks, bryozoans, echinoderms	
	22X-2, 73-76	200.03	Calcareous silty clay				
	24X-CC, 4-7	217.74	Sand				
	27X-4, 67-71	251.87	Calcareous silty clay				
	28X-1, 4-8	256.34	Wackestone			Benthic and planktonic foraminifers	
	35X-5, 78-81	330.68	Calcareous silty clay				
	37X-1, 112-114	344.21	Medium- to coarse-grained sandstone	Argillaceous/glassy	Andesites		
	180-1109D-						
	1R-2, 48-49	354.78	Medium-grained sandstone	Argillaceous/carbonatic		Planktonic foraminifers	
early Pliocene to middle Pliocene	1R-2, 56-58	354.86	Medium-grained sandstone	Carbonatic matrix	Andesites	Foraminifers	
	2R-2, 109-113	361.51	Fine- to medium-grained sandstone	Carbonatic matrix	Shards		
	3R-2, 148-149	371.68	Fine-grained sandstone	Glassy	Shards		
	4R-5, 59-62	383.36	Volcaniclastic sandy siltstone				
	4R-7, 0-2	385.53	Fine-grained sandstone	Argillaceous/carbonatic	Andesites		
	6R-2, 112-114	399.73	Fine-grained sandstone			Foraminifers	
	8R-1, 54-58	417.04	Wackestone				
	8R-3, 96-100	419.88	Wackestone and sandstone				
	9R-5, 24-26	431.76	Calcareous clay				
	10R-1, 132-134	436.95	Fine-grained sandstone				
	10R-4, 95-98	440.70	Fine-grained sandstone			Foraminifers	
	11R-3, 83-85	448.88	Fine-grained sandstone			Foraminifers	
	12R-4, 95-97	459.82	Fine-grained sandstone	Glassy	Shards		
	18R-4, 50-54	517.02	Calcareous silty claystone				
	20R-2, 104-108	534.51	Fine-grained sandstone				
	20R-5, 105-107	538.05	Siltstone		Andesites		
	22R-1, 57-60	551.77	Siltstone	Argillaceous		Planktonic foraminifers	
	22R-1, 102-104	552.22	Siltstone			Planktonic and benthic foraminifers, mollusks	
	23R-1, 125-128	562.05	Calcareous silty claystone				
	25R-6, 8-10	577.54	Packstone			Foraminifers, mollusks	
	27R-1, 45-48	590.05	Packstone			Benthic foraminifers, mollusks	
	27R-4, 64-68	593.73	Packstone-grainstone				
	28R-1, 8-11	599.28	Boundstone			Mollusks	
	30R-1, 6-10	618.56	Packstone-grainstone				
	32R-2, 101-103	640.32	Grainstone		Andesites	Echinoderms, mollusks, bryozoans	
	34R-1, 10-13	657.20	Packstone-grainstone				
	34R-5, 62-65	663.00	Packstone			Planktonic and benthic shells	

Table T3 (continued).

Age	Core, section, interval (cm)	Depth (mbsf)	Lithology	Matrix/Cement	Lithic fragments	Bioclasts	Organic carbon
?	35R-2, 122–125	669.04	Packstone-grainstone	Pelitic/carbonatic		mollusks, benthic and planktonic foraminifers, echinoids	
	36R-6, 51–54	684.41	Calcareous clayey siltstone				
	37R-2, 104–105	688.52	Fine-grained sandstone	Pelitic	Shards		X, as ribbons
	38R-2, 12–18	697.10	Fine-grained sandstone	Glassy			
	38R-2, 76–79	697.74	Lignite				X
	38R-4, 10–14	699.86	Fine-grained sandstone				
	39R-2, 135–139	707.96	Claystone			Foraminifers	X
	39R-3, 28–31	708.32	Fine-grained sandstone				
	39R-3, 64–67	708.68	Fine- to medium-grained sandstone				
	43R-2, 0–3	744.92	Clayey siltstone				X, as ribbons
	43R-3, 65–69	746.46	Diabase?				
	43R-3, 69–71	746.50	Diabase?	Argillaceous/glassy	Shards		
	44R-1, 6–8	753.66	Medium-grained sandstone				
	45R-1, 46–50	763.66	Orthoconglomerate	Sparry cement	Basalts, dolerites		
	45R-1, 86–89	764.06	Orthoconglomerate	Carbonatic matrix	Basalts		
	45R-1, 88–90	764.08	Conglomerate	Carbonatic matrix	Basalts, dolerites		
	45R-1, 107–110	764.27	Orthoconglomerate		Basalts		
	45R-2, 109–114	765.79	Orthoconglomerate	Glassy	Shards, basalts		

Notes: Lithic fragments: gabbro includes olivine gabbro, oxide gabbro, and diorite compositions; basalt and dolerite refer to tholeiitic serial affinity; andesite includes calc-alkaline basalt andesite and andesite to quartz andesite; felsite refers to dacite and rhyolite compositions; trachyte includes lava clasts and glass with K-feldspar microliths; granophyre indicates fine-grained eutectic quartz-feldspar intergrowth; shards include ash fall tephra or prevalent glassy matrix in turbidites; volcanics include fragments of uncertain definition. Prh = prehnite, Pmp = pumpellyite, X = present.

Table T4. Petrographic features of sediments from Woodlark Basin northern margin Site 1115. (See table notes. Continued on next page.)

Age	Core, section, interval (cm)	Depth (mbsf)	Lithology	Matrix/Cement	Lithic fragments	Bioclasts	Organic carbon
	180-1115B-						
Pleistocene	1H-5, 63–68	6.63	Siltstone				
	8H-5, 75–80	70.95	Siltstone				
	10H-4, 55–61.5	88.25	Siltstone				
late Pliocene	16H-1, 84–88	141.04	Siltstone				
	21H-4, 44–49	192.64	Siltstone				
early to middle Pliocene	23H-6, 44–47	214.64	Siltstone				
	27X-2, 11–15	246.61	Siltstone				
	28X-CC, 20–23	256.75	Siltstone			Foraminifers	
	29X-4, 17–24	268.97	Siltstone				
	30X-CC, 39–40	275.36	Siltstone				
	180-1115C-						
	1R-1, 67–71	283.87	Siltstone				
	2R-1, 17–19	292.97	Siltstone		Shards, volcanics, felsites	Planktonic foraminifers	
	5R-1, 40–42	322.13	Siltstone			Planktonic and benthic foraminifers	
	6R-2, 17–19	333.07	Fine-grained sandstone				
	6R-5, 114–116	338.54	Sandy siltstone		Volcanics, andesites		
	7R-2, 33–34	342.79	Sandy siltstone			Planktonic foraminifers	
	7R-3, 133–135	345.25	Sandy siltstone				
	8R-1, 64–66	351.24	Sandy siltstone				
	9R-2, 80–83	361.89	Clayey siltstone				
	10R-1, 5–7	369.55	Clayey siltstone		Volcanics, andesites	Planktonic and benthic foraminifers	
	11R-4, 57–58	383.99	Clayey siltstone		Volcanics, andesites	Planktonic and benthic foraminifers	
late Miocene	12R-4, 144–148	394.34	Clayey siltstone		Andesites		
	12R-5, 50–53	394.90	Clayey siltstone		Andesites		
	12R-6, 59–61	396.49	Clayey siltstone				
	13R-4, 140–143	403.55	Clayey siltstone			Benthic foraminifers	
	14R-2, 53–55	409.67	Clayey siltstone				
	14R-2, 68–70	409.82	Conglomerate		Andesites	Foraminifers, mollusks	
	15R-3, 79–83	421.09	Grainstone		Volcanics		X, inside tests
	16R-2, 4–7	427.73	Packstone				
	19R-CC, 8–10	456.10	Fine-grained sandstone	Carbonatic matrix			
	21R-3, 91–93	477.59	Wackestone			Benthic foraminifers	
	21R-4, 108–112	479.08	Fine- to medium-grained sandstone				
	22R-3, 104–105	487.80	Fine- to medium-grained sandstone	Carbonatic matrix			
	23R-1, 93–94	495.05	Fine- to medium-grained sandstone	Carbonatic matrix	Andesites	mollusks, benthic foraminifers, echinoderms	
	24R-3, 49–50	507.29	Fine-grained sandstone	Carbonatic matrix		Benthic foraminifers, mollusks	
	25R-2, 56–57	515.46	Fine- to medium-grained sandstone				
	26R-1, 8–9	523.08	Sandstone			Benthic foraminifers	
	27R-CC, 7–8	533.12	Silty sandstone	Carbonatic matrix		mollusks	
	29R-1, 72–73	552.52	Medium-grained sandstone	Sparry matrix	Shards, andesites, felsites, serpentinites		
	29R-1, 82–83	552.62	Fine-grained sandstone	Carbonatic matrix			
	29R-3, 10–13	554.39	Fine-grained sandstone				
	30R-3, 105–110	564.35	Fine-grained sandstone				
	30R-5, 45–48	566.46	Fine-grained sandstone				

Table T4 (continued).

Age	Core, section, interval (cm)	Depth (mbsf)	Lithology	Matrix/Cement	Lithic fragments	Bioclasts	Organic carbon
	30R-CC, 10–12	566.83	Medium-grained sandstone to conglomerate	Sparry matrix	Volcanics, andesites, granophyres, felsites, basalts, dolerites, gabbros, epidiosites	Algae	
middle Miocene	30R-CC, 16–19	566.89	Coarse-grained sandstone		Andesites, felsites		X
	31R-1, 94–96	571.94	Fine-grained sandstone				
	32R-1, 78–81	581.38	Fine-grained sandstone				
	32R-1, 138–140	581.98	Fine- to coarse-grained sandstone				
	32R-3, 52–55	583.49	Fine- to coarse-grained sandstone				
	33R-3, 68–71	593.74	Packstone	Carbonatic mud	Andesites	Benthic foraminifers	X
	34R-2, 124–126	602.52	Packstone	Carbonatic mud			
	35R-1, 85–88	610.25	Packstone	Carbonatic mud	Andesites	Benthic organisms	
	35R-4, 12–17	613.79	Silty claystone		Andesites, sandstones		
	35R-4, 102–105	614.69	Silty claystone	Pelitic/carbonatic		Benthic and planktonic foraminifers	X
	36R-1, 137–140	620.47	Silty claystone				
	36R-2, 25–27	620.75	Laminated sandstone			Foraminifers	
	37R-CC, 1–3	628.81	Fine-grained sandstone		Andesites, tephrites		
	39R-CC, 1–2	648.11					
	40R-2, 105–107	660.35	Siltstone				X
	42R-1, 26–28	677.36					
	42R-3, 138–141	680.78	Silty claystone	Pelitic		Planktonic foraminifers	
	43R-4, 111–115	692.14	Siltstone				X
	48R-2, 13–17	736.41	Clayey siltstone	Pelitic		Foraminifers, mollusks	X
	48R-3, 81–83	738.46					
50R-1, 18–21	754.48	Siltstone			Planktonic foraminifers	X	
51R-1, 119–120	765.09	Siltstone			Planktonic and benthic foraminifers	X	
52R-3, 61–71	776.76	Clayey siltstone			Planktonic foraminifers	X	
53R-3, 118–120	787.22	Packstone	Carbonatic mud	Shards, andesites	Benthic foraminifers, red algae		
53R-6, 42–45	790.35	Clayey siltstone	Carbonatic matrix		Planktonic and benthic foraminifers, mollusks		
54R-1, 94–98	793.74	Clayey siltstone	Carbonatic matrix				

Notes: Lithic fragments: gabbro includes olivine gabbro, oxide gabbro, and diorite compositions; basalt and dolerite refer to tholeiitic serial affinity; andesite includes calc-alkaline basalt andesite and andesite to quartz andesite; felsite refers to dacite and rhyolite compositions; trachyte includes lava clasts and glass with K-feldspar microliths; granophyre indicates fine-grained eutectic quartz-feldspar intergrowth; shards include ash fall tephra or prevalent glassy matrix in turbidites; volcanics include fragments of uncertain definition. Prh = prehnite, Pmp = pumpellyite, X = present.

Table T5. Petrographic features of sediments from Woodlark Basin northern margin Site 1118. (See table notes. Continued on next page.)

Age	Core, section, interval (cm)	Depth (mbsf)	Lithology	Matrix/Cement	Lithic fragments	Bioclasts	Organic carbon
	180-1118A-						
late Pliocene to Pleistocene	7R-1, 43–46	262.93	Fine-grained sandstone				
	13R-2, 31–33.5	322.11	Fine-grained sandstone				
	15R-5, 141–142	345.85	Fine-grained sandstone				
	20R-5, 15–18	393.20	Sandy siltstone			Planktonic foraminifers, mollusks	
middle Pliocene	22R-5, 94–98	412.87	Siltstone				
	24R-5, 105–107	432.23	Fine-grained sandstone/siltstone			Planktonic and benthic foraminifers	
	33R-2, 66–70	514.03	Fine-grained sandstone				
	34R-3, 61–63	525.12	Fine-grained sandstone	Argillaceous		Shell debris	X
	35R-1, 140–143	532.80	Fine-grained sandstone	Argillaceous		Foraminifers	
	36R-3, 8–10	543.72	Fine-grained sandstone	Argillaceous		Foraminifers	
	37R-3, 95–97	554.43	Siltstone		Andesites		
	38R-3, 128–130	564.40	Clayey siltstone				
	39R-3, 100–103	573.75	Siltstone				
	41R-3, 130–132	593.22	Laminated fine-grained sandstone and siltstone			Planktonic foraminifers, mollusks	
	42R-3, 112–114	602.43	Siltstone/sandstone		Andesites		
	43R-7, 63–64	616.90	Fine-grained sandstone	Carbonatic matrix		Benthic and planktonic foraminifers	
	44R-4, 129–130	623.45	Silty sandstone	Glassy	Shards	Shell debris	
	45R-4, 105–107	632.49	Silty sandstone	Argillaceous		Benthic and planktonic foraminifers, mollusks	
	46R-4, 99–101	642.54	Silty sandstone	Argillaceous/carbonatic		mollusks, planktonic foraminifers	
	47R-6, 128–130	654.94	Silty sandstone	Argillaceous/carbonatic		mollusks, planktonic foraminifers	
	53R-2, 60–63	706.70	Silty sandstone				
	56R-1, 44–47	734.24	Silty sandstone	Glassy	Shards		
	57R-2, 52–55	745.34	Silty sandstone				
	57R-4, 20–21	747.84	Fine- to medium-grained sandstone	Glassy	Shards	Benthic foraminifers, mollusks	
	58R-3, 38–40	756.05	Silty sandstone	Glassy	Shards	Foraminifers	
	58R-4, 52–56	757.33	Silty sandstone				
	58R-5, 18–20	758.49	Fine-grained sandstone				
	59R-2, 133–135	765.32	Fine-grained sandstone	Glassy	Shards		
	60R-1, 93–95	773.24	Siltstone		Volcanics	Foraminifers	X
	64R-1, 49–51	811.19	Laminated fine-grained sandstone and siltstone	Argillaceous		Foraminifers	X
	64R-1, 127–128	811.97	Fine- to medium-grained sandstone	Argillaceous	Andesites	Planktonic foraminifers	
	65R-4, 24–26	824.62	Fine-grained sandstone				
	66R-3, 31–34	833.05	Laminated fine-grained sandstone and siltstone		Andesites	Benthic foraminifers	
	66R-5, 17–21	835.77	Laminated fine-grained sandstone and siltstone		Andesites	Benthic and planktonic foraminifers	
early Pliocene	67R-4, 73–74	844.62	Medium-grained sandstone			Benthic foraminifers	
	68R-2, 117–120	851.92	Medium-grained sandstone			Benthic foraminifers, mollusks	
	68R-3, 24–28	852.30	Medium-grained sandstone	Argillaceous/carbonatic	Andesites	Foraminifers	X
	68R-3, 36–39	852.42	Coarse-grained sandstone	Glassy/carbonatic/sparry	Shards, andesites	Shell debris	
	68R-3, 102–105	853.08	Medium-grained sandstone	Glassy	Shards, andesites	Benthic foraminifers	
	68R-4, 31–33	853.87	Packstone	Argillaceous		mollusks, benthic foraminifers, echinoids, red algae	
?	69R-2, 68–72	861.18	Grainstone	Sparry	Dolerites, chlorite schists	Red algae	

Table T5 (continued).

Age	Core, section, interval (cm)	Depth (mbsf)	Lithology	Matrix/Cement	Lithic fragments	Bioclasts	Organic carbon
	69R-3, 58–61	862.55	Grainstone			Algae, foraminifers, mollusks, bryozoans	X, inside tests
	70R-1, 0–1	868.70	Grainstone		Volcanics, basalts	Shell debris, algae, mollusks	
	70R-1, 72–74	869.42					
	70R-3, 129–130	872.54	Fine-grained sandstone		Basalts		
	71R-1, 13–15	878.53	Conglomerate		Volcanics, basalts, dolerites, gabbros		
	71R-1, 29–31	878.69	Conglomerate		Basalts, gabbros		

Notes: Lithic fragments: gabbro includes olivine gabbro, oxide gabbro, and diorite compositions; basalt and dolerite refer to tholeiitic serial affinity; andesite includes calc-alkaline basalt andesite and andesite to quartz andesite; felsite refers to dacite and rhyolite compositions; trachyte includes lava clasts and glass with K-feldspar microliths; granophyre indicates fine-grained eutectic quartz-feldspar intergrowth; shards include ash fall tephra or prevalent glassy matrix in turbidites; volcanics include fragments of uncertain definition. X = present.

Table T6. Mineral compositions of the matrix of arenitic-siltitic sediments. (See table notes. Continued on next page.)

Core, section, interval (cm)	Depth (mbsf)	XRD identification: major (minor) constituents
180-1108B-		
1R-2, 57–63	1.57	Cal (Qtz, Am, Plg)
10R-1, 84–86	82.74	Plg, Qtz (Srp, Am)
16R-CC, 4–6	142.08	Cal, Kf (Arg, Am)
19R-3, 6–9	169.86	Cal (Qtz, Kf, Am)
27R-5, 66–70	251.56	Qtz, Plg (Am, Srp, Px, Sap)
28R-4, 68–70	258.77	Plg, Qtz (Am, Srp)
29R-1, 54–58	264.64	Plg, Qtz (Am, Srp)
44R-1, 128–131	409.48	Plg, Qtz, Cal (Sap, Am)
180-1109C-		
2H-4, 17–20	12.07	Am (Cal, Plg)
4H-5, 81–83.5	33.21	Cal (Qtz, Arg, Am)
4H-5, 85.5–88.5	33.26	Cal (Qtz, Arg, Am, Srp)
5H-2, 115–117	38.55	Cal (Arg, Qtz, Am, Plg)
5H-5, 29–31	42.19	Cal (Qtz, Srp, Plg, Hem)
7H-3, 23–25	58.13	Cal (Qtz, Plg, Hem)
9H-6, 11.5–17.5	81.51	Cal (Arg, Qtz, Am, Hem, Plg)
11H-7, 36–39	101.76	Cal (Arg, Am, Qtz)
12X-4, 115–118	108.05	Cal, Qtz, Plg, Sap, Am (Srp, Ill, Tlc)
18X-1, 67–69	160.77	Qtz, Cal (Ill, Srp, Plg, Tlc, Sap)
22X-2, 73–76	200.03	Cal, Plg, Am (Qtz, Sap, Tlc)
24X-CC, 4–7	217.74	Plg, Qtz (Srp, CAm, Tlc, An)
27X-4, 67–71	251.87	Cal (Am, Qtz, Plg, Arg, Dol)
35X-5, 78–81	330.68	Cal (Qtz, Plg, WM, Am, Sap)
180-1109D-		
4R-5, 59–62	383.36	Dol (Plg, Qtz, Am, Hem, WM)
9R-5, 24–26	431.76	Cal (Plg, Qtz, Sap, Ill)
18R-4, 50–54	517.02	Cal (Plg, Qtz, Sap, Ill)
23R-1, 125–128	562.05	Cal, Plg (Qtz, Am, Arg)
27R-4, 64–68	593.73	Cal (Am, Plg)
30R-1, 6–10	618.56	Cal, Qtz (Plg, Am)
34R-1, 10–13	657.20	Cal, Plg (Ank, Am, Qtz)
35R-2, 122–125	669.04	Cal (Am, Srp, Hem, Arg, Qtz)
36R-6, 51–54	684.41	Cal, Plg, Dol (Qtz, Sap, Srp)
38R-2, 76–79	697.74	Bass, Pyr, Gp
39R-2, 135–139	707.96	Plg (Sap, Pyr, Qtz)
43R-2, 0–3	744.92	Sap (Plg)
43R-3, 65–69	746.46	Sap (Plg, Qtz, Dol)
43R-3, 69–71	746.50	Sap (Plg)
180-1110A-		
1H-3, 52–54	3.52	Cal (Qtz, Am, Plg)
180-1111A-		
8R-2, 77–81	68.47	Qtz, Plg (Am)
13R-2, 89–93	118.05	Cal (Qtz, Hem, Am)
180-1112A-		
1R-2, 20–23	1.70	Cal (Qtz, Plg, CAm)
180-1114A-		
1R-CC, 1–6	0.01	Cal (Qtz, Arg, Am)
6R-2, 68–72	46.65	Qtz, Plg (Am)
12R-1, 88–91	104.08	Cal (Plg, Srp Qtz, Sap)
30R-1, 47–51	276.57	Qtz, Plg (Am)
31R-1, 15–17	285.95	Cal, Qtz (Plg, Am)
180-1115B-		
1H-5, 63–68	6.63	Cal (Arg, Am, Qtz)
8H-5, 75–80	70.95	Cal (Arg, Plg, Am, Qtz)
10H-4, 55–61.5	88.25	Ank, Qtz (WM, Plg)
16H-1, 84–88	141.04	Cal (Qtz, Plg)
21H-4, 44–49	192.64	Cal (Plg, Qtz, Am)
23H-6, 44–47	214.64	Cal (Plg, Qtz, WM, Am)
27X-2, 11–15	246.61	Plg (Qtz, Cal, Pyr, Am, WM, Hem)
29X-4, 17–24	268.97	Plg (Cal, Qtz, WM, Sap)
180-1115C-		
1R-1, 67–71	283.87	WM (Qtz, Cal, Plg)

Table T6 (continued).

Core, section, interval (cm)	Depth (mbsf)	XRD identification: major (minor) constituents
7R-3, 133–135	345.25	Cal (Qtz, Plg)
8R-1, 64–66	351.24	Cal (Qtz, Plg, WM, Am)
9R-2, 80–83	361.89	Plg (Cal, Qtz, Sap, Am, Arg)
12R-6, 59–61	396.49	Cal (Plg, Qtz, Sap, Ill, Hem)
14R-2, 53–55	409.67	Plg (Cal, Am, Ill, Qtz, Hem)
21R-4, 108–112	479.08	Cal (Plg, Am, Qtz, WM, Hem)
29R-3, 10–13	554.39	Plg (Qtz, Sap, Kln)
34R-2, 124–126	602.52	Cal (Sap, Plg)
42R-1, 26–28	677.36	Cal (Plg, Qtz, Sap, Arg, Pyr)
48R-3, 81–83	738.46	Plg (Cal, Sap, Qtz)
53R-3, 118–120	787.22	Cal (Plg, Sap)
180-1116A-		
5R-1, 18–20	33.98	Plg (Qtz, Cal, Am, Sap)
9R-1, 122.5–126	63.83	Qtz, Cal (Plg, Zeol, Am)
16R-3, 6–8	132.22	Cal (Plg, Qtz, Sep, Am)
180-1118A-		
7R-1, 43–46	262.93	Cal (Plg, Qtz, Arg, Am)
13R-2, 31–33.5	322.11	Cal (Plg, Qtz, Am)
22R-5, 94–98	412.87	Cal (Qtz, Plg, Am)
33R-2, 66–70	514.03	Cal (Plg, Qtz, Sap, Am, Rect)
39R-3, 100–103	573.75	Plg (Qtz, Dol, Am, Cal, WM)
41R-3, 130–132	593.22	Cal (Qtz, Sap, Plg)
53R-2, 60–63	706.70	Plg, WM (Am)
57R-2, 52–55	745.34	Plg (Am, Ill, Qtz, Hem)
58R-4, 52–56	757.33	Plg, WM (Pyr, Am)
58R-5, 18–20	758.49	Cal (Qtz, Plg, Sap)
65R-4, 24–26	824.62	Cal (Qtz, Plg)
68R-4, 31–33	853.87	Cal (Qtz, Plg, Dol)

Notes: Am = amphibole, Ank = ankerite, Arg = aragonite, Bass = bassanite, Ca-Am = calcium amphibole, Cal = calcite, Chl = chlorite, Crs = cristobalite, Dol = dolomite, Gp = gypsum, Hbl = hornblende, Hem = hematite, Ill = illite, Na-Am = sodium amphibole, Kf = K-feldspar, Kln = kaolinite, Pl = plagioclase, Px = pyroxene, Py = pyrite, Qtz = quartz, Rt = rutile, Sap = saponite, Sep = sepiolite, Tlc = talc, WM = white mica, Zeol = zeolite. Components in parentheses are minor constituents.

Table T7. Clay mineral composition of samples with high mud matrix.

Core, section, interval (cm)	Depth (mbsf)	XRD identification: major (minor) constituents
180-1108B-		
27R-5, 66-70	251.56	Sap, Qtz (Pl, Am, Srp, WM)
44R-1, 128-131	409.48	Sap (Chl)
180-1109C-		
12X-4, 115-118	108.05	Tlc (Sap, Chl, Bt, Am, Srp)
18X-1, 67-69	160.77	Tlc Sap, Srp, (WM, Chl)
22X-2, 73-76	200.03	Sap (Ca-Am, Chl, Srp, Tlc, Ill)
35X-5, 78-81	330.68	Ill (Sap, Srp, Tlc, Chl)
180-1109D-		
9R-5, 24-26	431.76	Sap (Ca-Am, Ill, Srp)
18R-4, 50-54	517.02	Sap (Srp, Ill)
36R-6, 51-54	684.41	Sap (Chl)
39R-2, 135-139	707.96	Sap
43R-2, 0-3	744.92	Sap
43R-3, 65-69	746.46	Sap
43R-3, 69-71	746.50	Sap (Pl, Na-Am)
180-1115C-		
9R-2, 80-83	361.89	Sap (Na-Am, Pl, WM)
12R-6, 59-61	396.49	Sap (Am, Ill)
29R-3, 10-13	554.39	Sap
34R-2, 124-126	602.52	Sap
42R-1, 26-28	677.36	Sap (Chl)
48R-3, 81-83	738.46	Sap (Chl)
53R-3, 118-120	787.22	Sap
180-1116A-		
5R-1, 18-20	33.98	Sap (Chl)
16R-3, 6-8	132.22	Sap (Srp, Pl, Chl)
180-1118A-		
33R-2, 66-70	514.03	Sap (Chl, Tlc, Chl)
41R-3, 130-132	593.22	Sap (Chl)
58R-5, 18-20	758.49	Sap (Chl, WM)

Notes: Am = amphibole, Bt = biotite, Ca-An = calcium amphibole, Chl = chlorite, Ill = illite, Na-Am = sodium amphibole, Pl = plagioclase, Qtz = quartz, Sap = saponite, Srp = serpentine, Tlc = talc, WM = white mica.

Table T8. Organic carbon content in selected pelite samples.

Hole, core, section, interval (cm)	Organic carbon (wt%)
180-1108B- 45R-CC, 6.0–9.0	15.01
180-1109D- 38R-2, 76.0–79.0	0.98
38R-CC, 7.5–9.5	0.15
39R-2, 135.0–139.0	0.21
180-1112A- 1R-2, 20.0–23.0	0.54
180-1114A- 11R-CC, 19.0–24.0	0.17
22R-1, 77.0–80.0	0.88
180-1105C- 43R-4, 51.0–53.0	0.18
180-1115C- 31R-CC, 16.0–18.0	10.08
52R-4, 1.0–4.0	0.40
60R-1, 58.0–60.0	1.07
180-1118A- 34R-4, 44.0–46.0	0.42
69R-2, 68.0–72.0	0.12

Table T9. Chemical composition of glass shards and groundmass of volcanic clasts.

Sample:	Northern margin										Footwall	
	180-1118A-68R-3, 24–28 cm					180-1108B-3R-1, 41–44.5 cm					180-1114A-28R-CC, 3–5 cm	180-1116A-6R-1, 37–39 cm
Phenocrysts:	Bt, Plg (An13), Hbl, Kf (Or62)		Plg (An13), Hbl		Plg (An48–51)		Cpx, Plg (An43–50)		Plg (An11), Kf (Or94)		Plg (An45), Cpx	Plg (An51), Ilm
Microliths:					Plg (An46)		Plg (An46)		Plg (An40)			
Major element oxide (wt%):												
SiO ₂	76.80	77.21	69.12	61.19	52.37	55.53	53.27	51.97	50.78	54.46	58.12	63.84
TiO ₂	0.18	0.09	0.47	0.80	0.63	0.74	0.96	0.68	0.98	0.74	2.41	1.21
Cr ₂ O ₃	0.42	0.22	2.46	0.87	1.18	0.57	0.60	0.84	0.98	0.60	3.57	0.30
Al ₂ O ₃	13.49	13.64	10.03	17.62	8.95	5.69	7.22	11.71	12.75	7.19	10.63	14.13
Fe ₂ O ₃	0.61	0.87	2.81	8.25	12.75	12.77	11.86	10.10	9.77	10.73	9.66	4.47
FeO	0.00	0.00	0.00	0.00	0.00	0.00	0.00	0.00	0.00	0.00	0.00	0.00
MnO	0.07	0.07	0.04	0.10	0.12	0.05	0.02	0.09	0.14	0.10	0.15	0.11
MgO	0.00	0.00	4.15	6.76	19.10	19.93	21.12	17.43	17.07	21.43	10.20	3.13
NiO	0.02	0.03	0.00	0.01	0.09	0.19	0.08	0.09	0.02	0.11	0.00	0.00
CaO	1.14	1.22	6.57	2.35	2.82	3.71	3.82	4.60	4.74	3.55	3.28	2.25
Na ₂ O	2.46	1.86	3.04	0.66	0.90	0.53	0.43	0.44	0.46	0.50	0.77	3.95
K ₂ O	4.80	4.79	1.32	1.38	1.09	0.28	0.63	2.05	2.30	0.57	1.22	6.61

Note: An = anorthite, Bt = biotite, Cpx = clinopyroxene, Hbl = hornblende, Ilm = ilmenite, Kf = K-feldspar, Or = orthoclase, Plg = plagioclase.

Table T10. Representative analyses of clinopyroxene phenocrysts.

Sample (matrix):	180-1114A-28R-CC, 3–5 cm (Cpx)		180-1114A-28R-CC, 3–5 cm (Opx)		180-1116A-6R-1, 37–39 cm	180-1108B-3R-1, 41–44.5 cm			180-1108B-41R-1,180-1108B-47R-1, 75–78 cm 33–37.5 cm		
Analysis number:	1	2	3	4	1	1	2	3	1	1	
Major element oxide (wt%):											
SiO ₂	51.42	51.64	53.85	57.66	50.34	53.18	50.76	51.40	50.66	53.16	
TiO ₂	0.80	0.83	0.42	0.18	1.03	0.51	0.91	1.01	0.95	0.80	
Cr ₂ O ₃	0.61	0.30	0.20	0.27	0.23	0.62	0.51	0.35	0.33	1.22	
Al ₂ O ₃	2.22	1.91	1.90	25.71	2.03	1.10	2.29	1.78	1.91	0.20	
Fe ₂ O ₃	7.66	7.28	2.34	0.00	4.03	2.07	4.04	6.08	1.88	2.40	
FeO	0.00	2.05	13.64	0.84	9.21	3.20	4.81	2.66	6.49	1.80	
MnO	0.29	0.30	0.43	0.13	0.46	0.24	0.24	0.28	0.29	0.05	
MgO	16.51	16.15	27.32	0.00	15.08	19.15	15.75	16.23	15.63	17.34	
NiO	0.17	0.16	0.05	0.13	0.15	0.00	0.12	0.19	0.00	0.07	
CaO	21.25	20.45	1.36	8.18	18.68	20.24	20.93	20.57	20.53	24.13	
Na ₂ O	1.20	0.94	0.00	5.71	0.00	0.00	0.23	0.77	0.00	0.00	
K ₂ O	0.22	0.21	0.07	1.07	0.16	0.18	0.13	0.13	0.16	0.18	
Total:	102.35	102.23	101.57	99.88	101.4	100.49	100.71	101.45	98.83	101.35	
Cation (atoms/formula unit):											
Si	1.848	1.870	1.916	2.088	1.870	1.929	1.872	1.875	1.903	1.927	
Ti	0.022	0.023	0.011	0.005	0.028	0.014	0.025	0.027	0.027	0.022	
Cr	0.017	0.008	0.005	0.007	0.007	0.018	0.015	0.011	0.009	0.035	
Al	0.094	0.082	0.079	1.097	0.089	0.047	0.099	0.076	0.085	0.008	
Fe ³⁺	0.207	0.198	0.063	0.000	0.113	0.057	0.112	0.167	0.053	0.066	
Fe ²⁺	0.000	0.063	0.406	0.025	0.286	0.097	0.148	0.081	0.204	0.055	
Mn	0.008	0.009	0.013	0.004	0.014	0.007	0.007	0.008	0.009	0.002	
Mg	0.885	0.872	1.449	0.000	0.835	1.035	0.866	0.882	0.875	0.937	
Ni	0.005	0.005	0.001	0.004	0.004	0.000	0.004	0.005	0.000	0.002	
Ca	0.818	0.794	0.052	0.317	0.744	0.786	0.827	0.804	0.826	0.937	
Na	0.084	0.066	0.000	0.401	0.000	0.000	0.016	0.054	0.000	0.000	
K	0.011	0.009	0.003	0.049	0.007	0.008	0.006	0.006	0.007	0.008	
Mineral composition (mol%):											
Enstatite:	0.445	0.438	0.699	0.002	0.420	0.518	0.435	0.444	0.438	0.470	
Ferrosilite:	0.000	0.031	0.196	0.013	0.143	0.048	0.074	0.041	0.102	0.027	
Wollastonite:	0.373	0.367	0.026	0.159	0.342	0.377	0.377	0.378	0.384	0.467	
Other:	0.182	0.164	0.079	0.826	0.095	0.057	0.114	0.137	0.076	0.036	

Note: Cpx = clinopyroxene, Opx = orthopyroxene.

Table T11. Representative analyses of biotite phenoclasts.

Sample:	180-1118A-68R-3, 24–28 cm		180-1116A-6R-1, 37–39 cm		180-1108B-33R-1, 41–44.5 cm
Analysis number:	1	2	1	2	1
Occurrence:	Phenoclast	Phenoclast	Phenoclast	Phenoclast	Phenoclast
Major element oxide (wt%):					
SiO ₂	37.24	37.77	37.39	37.48	38.02
TiO ₂	3.42	3.30	4.40	4.17	4.89
Cr ₂ O ₃	0.25	0.22	0.34	0.22	0.32
Al ₂ O ₃	14.41	14.67	14.69	14.81	14.45
Fe ₂ O ₃	0.00	0.00	0.00	0.00	0.00
FeO	15.24	15.38	13.97	13.57	10.12
MnO	0.25	0.24	0.25	0.23	0.14
MgO	14.75	14.77	16.48	16.24	18.49
NiO	0.08	0.09	0.17	0.11	0.13
CaO	0.29	0.12	0.25	0.17	0.27
Na ₂ O	0.00	0.65	0.90	0.86	0.32
K ₂ O	9.42	9.52	8.98	9.19	9.78
H ₂ O	3.94	3.98	4.06	4.03	4.08
Total:	99.29	100.71	101.88	101.08	101.01
Cation (atoms/formula unit):					
Si	2.833	2.847	2.758	2.788	2.794
Ti	0.195	0.187	0.244	0.233	0.271
Cr	0.015	0.013	0.019	0.013	0.018
Al	1.299	1.303	1.277	1.298	1.251
Fe ²⁺	0.969	0.969	0.862	0.844	0.622
Mn	0.016	0.015	0.015	0.014	0.008
Mg	1.672	1.659	1.812	1.801	2.025
Ni	0.005	0.005	0.01	0.006	0.007
Ca	0.024	0.009	0.019	0.014	0.022
Na	0.000	0.095	0.128	0.124	0.045
K	0.914	0.915	0.845	0.872	0.917
OH ⁻	2.000	2.000	2.000	2.000	2.000

Table T12. Representative analyses of amphibole phenocrysts and phenoclasts.

Sample:	Rift basin						Footwall	Northern margin				
	180-1108B-3R-1, 41–44.5 cm			180-1108B-41R-1, 75–78 cm		180-1108B-47R-1, 33–37.5 cm	180-1116A-6R-1, 37–39 cm	180-1118A-68R-3, 24–28 cm				
Analysis number:	1	2	3	4	5	7	1	1	1	1		
Occurrence:	Hbl + Plg	Hbl + Opx	Hbl in qtz-vein	Hbl + Bt intergrowth		Red Hbl core	Hbl phenoclast	Red Hbl	Hbl	Hbl alt chl	Hbl + Bt	Hbl + Bt
Major element oxide (wt%):												
SiO ₂	48.36	46.49	51.42	44.55	43.12	51.88	42.35	43.27	46.46	43.94	49.57	
TiO ₂	1.27	0.95	0.56	2.51	3.68	0.56	3.56	2.39	0.96	1.97	0.9	
Cr ₂ O ₃	0.51	0.17	0.26	0.36	0.42	0.3	0.27	0.38	0.24	0.32	0.38	
Al ₂ O ₃	7.22	7.54	4.54	10.94	11.21	4.36	10.06	10.31	4.24	10.35	6.29	
Fe ₂ O ₃	4.37	4.54	9.02	0	0.53	7.4	4.23	4.16	9.09	5.52	2.52	
FeO	5.98	11.54	2.01	9.6	10.94	2.92	8.17	6.66	15.49	7.75	9.21	
MnO	0.33	0.39	0.4	0.29	0.3	0.19	0.22	0.18	0.37	0.31	0.49	
MgO	16.46	12.62	17.98	15.02	13.5	17.97	13.85	14.94	9.04	14.38	15.4	
NiO	0.17	0	0.13	0.14	0.15	0.11	0.11	0.08	0.06	0.05	0.11	
CaO	11.85	12.15	11.99	11.73	12.14	11.88	11.37	11.92	10.04	11.46	11.93	
Na ₂ O	1.87	1.29	0.52	3.67	2.22	0.66	2.33	2.33	1.73	2.83	1.8	
K ₂ O	0.68	0.52	0.4	0.95	1.27	0.28	0.97	0.54	0.82	1.05	0.68	
H ₂ O	2.11	2.04	2.15	2.08	2.06	2.14	2.03	2.05	1.98	2.08	2.1	
Total:	101.18	100.23	101.37	101.84	101.55	100.64	99.51	99.2	100.52	102	101.38	
Cation (atoms/formula unit):												
Si	6.873	6.834	7.179	6.407	6.624	7.274	6.254	6.341	7.023	6.330	7.080	
Ti	0.136	0.105	0.059	0.272	0.402	0.059	0.395	0.263	0.109	0.213	0.097	
Cr	0.057	0.020	0.029	0.041	0.048	0.033	0.032	0.044	0.029	0.036	0.043	
Al	1.209	1.306	0.747	1.854	1.919	0.721	1.751	1.780	0.755	1.757	1.058	
Fe ³⁺	0.467	0.502	0.948	0.000	0.058	0.780	0.470	0.459	1.034	0.598	0.271	
Fe ²⁺	0.711	1.418	0.234	1.154	1.329	0.342	1.008	0.816	1.958	0.933	1.099	
Mn	0.040	0.049	0.047	0.035	0.037	0.023	0.028	0.022	0.047	0.038	0.059	
Mg	3.487	2.765	3.742	3.219	2.923	3.755	3.048	3.263	2.036	3.087	3.278	
Ni	0.019	0.000	0.015	0.016	0.018	0.012	0.013	0.009	0.007	0.006	0.013	
Ca	1.804	1.913	1.793	1.807	1.889	1.784	1.799	1.871	2.626	1.768	1.825	
Na	0.515	0.368	0.141	1.023	0.625	0.179	0.667	0.662	0.507	0.791	0.499	
K	0.123	0.098	0.071	0.174	0.235	0.050	0.183	0.101	0.158	0.193	0.124	
OH ⁻	2.000	2.000	2.000	2.000	2.000	2.000	2.000	2.000	2.000	2.000	2.000	

Note: Bt = biotite, Chl = chlorite, Hbl = hornblende, Plg = plagioclase, Opx = orthopyroxene.

Table T13. Representative analyses of plagioclase microliths, phenocrysts, and phenoclasts.

Sample:	180-1114A-28R-CC, 3–5 cm						180-1116A-6R-1, 37–39 cm		180-1108B-3R-1, 41–44.5 cm								180-1108B-41R-1, 75–78 cm		180-1108B-47R-1, 33–37.5 cm	
Analysis number:	1	2	3	4	5	6	1	2	1	2	3	4	5	6	7	8	1	2	1	2
Major element oxide (wt%):																				
SiO ₂	56.64	57.08	58.78	56.21	56.04	56.92	53.87	55.12	60.68	55.14	56.66	55.28	55.81	57.33	65.21	64.75	55.11	56.41	52.02	67.59
TiO ₂	0.23	0.33	0.62	0.19	0.32	0.11	0.21	0.15	0.16	0.19	0.16	0.29	0.18	0.25	0.16	0.22	0.18	0.17	0.16	0.03
Cr ₂ O ₃	0.30	0.33	0.35	0.25	0.25	0.23	0.27	0.24	0.28	0.26	0.13	0.33	0.23	0.23	0.22	0.20	0.19	0.21	0.29	0.13
Al ₂ O ₃	26.99	25.73	24.20	26.61	26.90	26.84	28.08	27.26	24.12	27.21	27.16	26.79	26.51	26.04	21.06	18.54	27.31	27.31	29.62	20.74
Fe ₂ O ₃	0.54	0.40	0.00	0.00	0.00	0.00	0.00	0.00	0.00	0.00	0.00	0.00	0.91	0.45	0.00	0.00	0.00	0.00	0.00	0.16
FeO	0.14	0.35	1.54	0.75	0.81	0.59	1.18	0.65	0.45	0.93	0.54	0.74	0.00	0.39	0.70	0.31	0.67	0.44	0.62	0.00
MnO	0.08	0.10	0.17	0.04	0.14	0.10	0.13	0.04	0.06	0.07	0.00	0.14	0.10	0.13	0.07	0.11	0.04	0.13	0.15	0.08
MgO	0.00	0.00	0.00	0.00	0.00	0.00	0.00	0.00	0.00	0.00	0.00	0.00	0.00	0.00	0.00	0.00	0.00	0.00	0.00	0.00
NiO	0.03	0.11	0.13	0.09	0.11	0.02	0.03	0.02	0.10	0.06	0.00	0.15	0.04	0.12	0.15	0.12	0.07	0.03	0.22	0.00
CaO	9.19	8.11	7.54	9.34	9.62	9.11	11.48	10.58	6.09	10.19	9.71	10.01	9.60	8.94	2.21	0.19	10.24	9.29	12.95	1.28
Na ₂ O	5.72	5.84	5.50	5.38	4.87	5.24	4.47	5.03	6.98	4.58	5.14	4.65	5.72	5.90	9.71	0.51	4.75	5.65	3.32	11.46
K ₂ O	0.89	1.35	1.29	0.71	0.92	0.98	0.22	0.63	1.54	0.74	0.87	0.94	0.77	0.88	0.42	15.65	0.69	0.52	0.32	0.17
Total:	100.74	99.73	100.12	99.57	99.98	100.14	99.94	99.72	100.46	99.37	100.37	99.32	99.87	100.67	99.91	100.60	99.25	100.16	99.67	101.64
Cation (ppm):																				
Si	2.539	2.584	2.672	2.552	2.547	2.573	2.455	2.504	2.709	2.525	2.556	2.532	2.524	2.573	2.890	2.983	2.521	2.541	2.930	2.909
Ti	0.008	0.011	0.021	0.007	0.011	0.004	0.007	0.005	0.005	0.007	0.005	0.010	0.006	0.008	0.005	0.008	0.006	0.006	0.006	0.001
Cr	0.011	0.012	0.013	0.009	0.009	0.008	0.010	0.009	0.010	0.009	0.005	0.012	0.008	0.008	0.008	0.007	0.007	0.008	0.011	0.004
Al	1.426	1.373	1.297	1.426	1.441	1.430	1.508	1.459	1.269	1.468	1.442	1.446	1.413	1.377	1.100	1.006	1.472	1.450	1.604	1.052
Fe ³⁺	0.018	0.014	0.000	0.000	0.000	0.000	0.000	0.000	0.000	0.000	0.000	0.000	0.031	0.015	0.000	0.000	0.000	0.000	0.000	0.005
Fe ²⁺	0.005	0.013	0.059	0.029	0.031	0.022	0.045	0.025	0.017	0.036	0.020	0.028	0.000	0.015	0.026	0.012	0.026	0.017	0.024	0.000
Mn	0.003	0.004	0.007	0.002	0.005	0.004	0.005	0.002	0.002	0.003	0.000	0.005	0.004	0.005	0.003	0.004	0.002	0.005	0.006	0.003
Mg	0.000	0.000	0.000	0.000	0.000	0.000	0.000	0.000	0.000	0.000	0.000	0.000	0.000	0.000	0.000	0.000	0.000	0.000	0.000	0.000
Ni	0.001	0.004	0.005	0.003	0.004	0.001	0.001	0.001	0.004	0.002	0.000	0.006	0.002	0.004	0.005	0.004	0.003	0.001	0.008	0.000
Ca	0.441	0.394	0.367	0.455	0.469	0.441	0.561	0.515	0.291	0.500	0.469	0.491	0.465	0.430	0.105	0.009	0.502	0.449	0.638	0.059
Na	0.497	0.513	0.485	0.474	0.429	0.459	0.395	0.443	0.604	0.407	0.450	0.413	0.502	0.513	0.834	0.046	0.421	0.494	0.296	0.957
K	0.051	0.078	0.075	0.041	0.053	0.057	0.013	0.037	0.088	0.043	0.050	0.055	0.044	0.050	0.024	0.920	0.040	0.030	0.019	0.009
Mineral composition (mol%):																				
Albite:	0.502	0.521	0.523	0.489	0.451	0.480	0.408	0.445	0.615	0.428	0.464	0.431	0.496	0.517	0.866	0.047	0.437	0.508	0.311	0.933
Anorthite:	0.446	0.400	0.396	0.469	0.493	0.461	0.579	0.518	0.296	0.526	0.484	0.512	0.460	0.433	0.109	0.010	0.521	0.461	0.670	0.058
Orthoclase:	0.051	0.079	0.081	0.042	0.056	0.059	0.013	0.037	0.089	0.046	0.052	0.057	0.044	0.051	0.025	0.944	0.042	0.031	0.020	0.009

Plate P1. Optical photomicrographs. 1. Epiclastic level with phenoclasts of embayed quartz, green hornblende, and biotite. The groundmass is composed of reworked glass shards (Sample 180-1118A-68R-3, 102–105 cm; plane-polarized light; scale bar = 0.1 mm). 2. Mud clasts with reworked planktonic foraminifer tests in fine-grained arenite (Sample 180-1118A-41R-3, 130–132 cm; plane-polarized light; scale bar = 0.5 mm). 3. Mud clasts with planktonic and benthic foraminifer tests in arenite enriched in volcaniclastic fragments. Note the abundant reworked benthic foraminifer tests (Sample 180-1108B-31R-2, 20.5–23.5 cm; plane-polarized light; scale bar = 1 mm). 4. Polygenic arenite with granite, epidote, serpentinite, and volcaniclastic materials. The cement is carbonaceous (Sample 180-1108B-3R-CC, 0–4 cm; crossed polars; scale bar = 0.5 mm). 5. Siltite and arenaceous levels with erosional structures (Sample 180-1116A-18R-2, 11–15 cm; plane-polarized light; scale bar = 1 mm). 6. Load cast textures at the contact between arenite and siltite (Sample 180-1118A-66R-5, 17–21 cm; plane-polarized light; scale bar = 0.5 mm). Bt = biotite, e = epidote, γ = granite, Hbl = hornblende, Qtz = quartz.

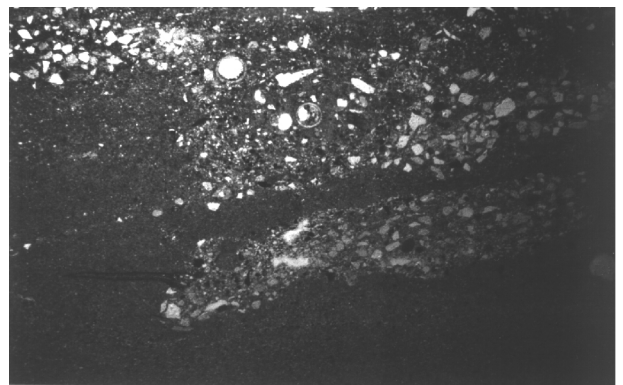
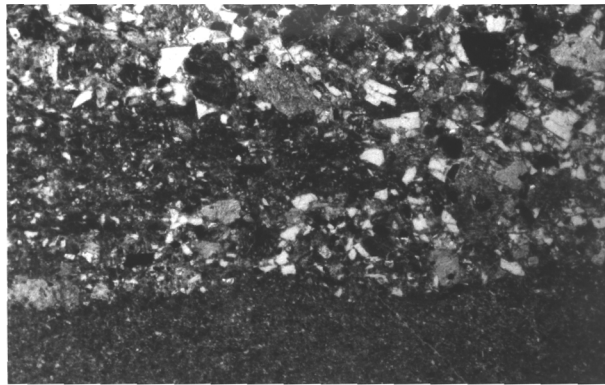
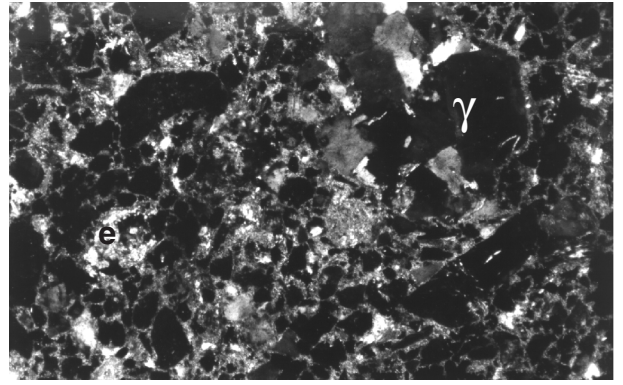
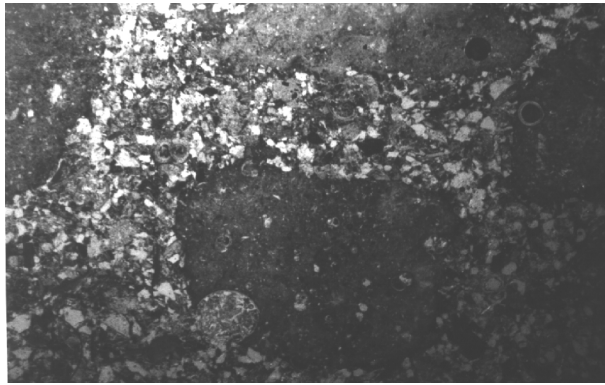
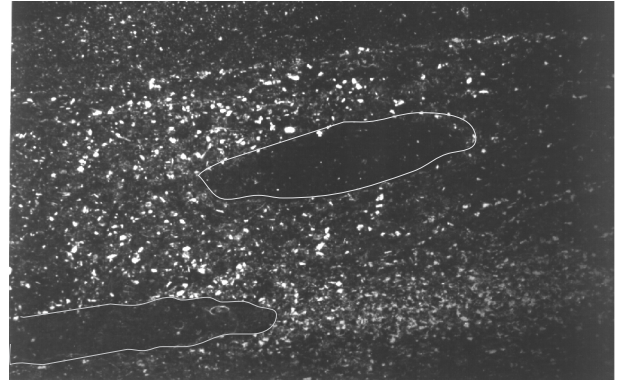
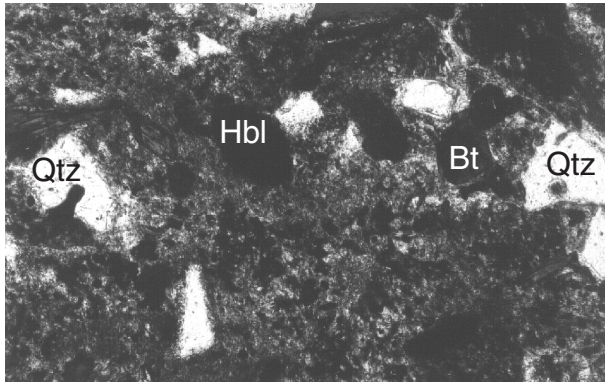
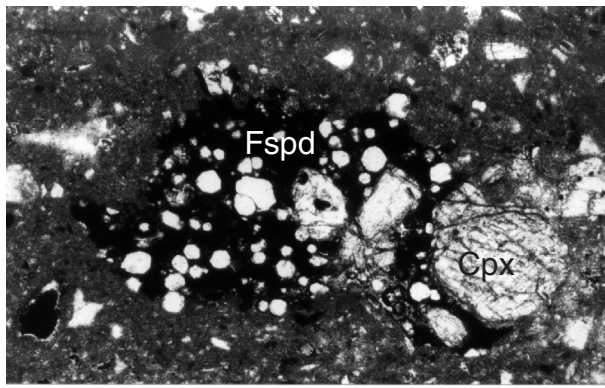
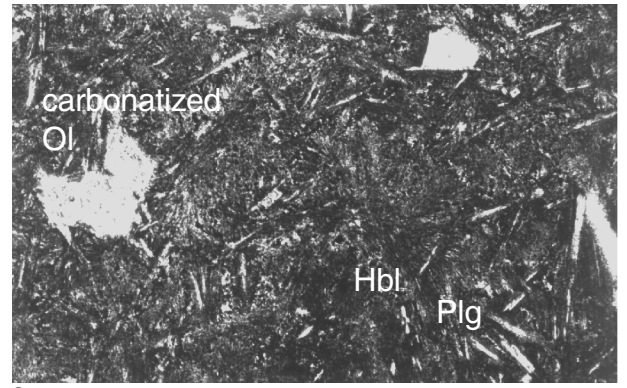


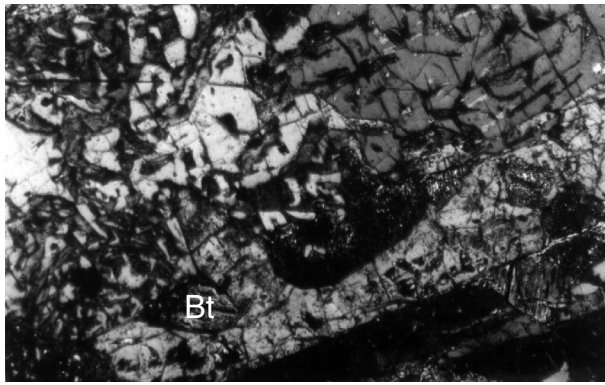
Plate P2. Optical photomicrographs. 1. Poorly rounded tephrite lava clast. The phenocrysts are zoned aegirine-augite and feldspathoid (noseana-sodalite series) (Sample 180-1115C-37R-CC, 1.0–3.0 cm; plane-polarized light; scale bar = 0.1 mm). 2. Tholeiitic basalt with phenocrysts of olivine (altered to calcite), skeletal plagioclase microcrysts, and groundmass with arborescent plagioclase (Sample 180-1108B-47R-CC, 5–7 cm; plane-polarized light; scale bar = 0.1 mm). 3. Rounded granite clast with eutectic quartz/K-feldspar texture and partially chloritized biotite (Sample 180-1108B-47R-1, 33–37.5 cm; crossed polars; scale bar = 0.5 mm). 4. Clast of calc-alkaline basaltic andesite in cryptocrystalline matrix. The phenocrysts are red hornblende and plagioclase (Sample 180-1115C-53R-3, 118–120 cm; plane-polarized light; scale bar = 0.5 mm). 5. Clast of calc-alkaline basalt andesite. The phenocrysts are zoned clinopyroxene and plagioclase in microcrystalline matrix (Sample 180-1115C-53R-3, 118–120 cm; plane-polarized light; scale bar = 0.5 mm). 6. Clast of calc-alkaline basaltic andesite. The phenocrysts are zoned red to red-brown hornblende, biotite, and plagioclase in microcrystalline groundmass (Sample 180-1115C-53R-3, 118–120 cm; plane-polarized light; scale bar = 0.1 mm). Bt = biotite, Cpx = clinopyroxene, Fspd = feldspathoid, Hbl = hornblende, Plg = plagioclase, Ol = olivine.



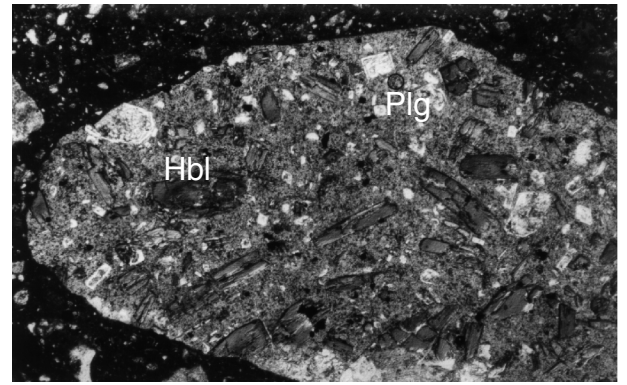
1



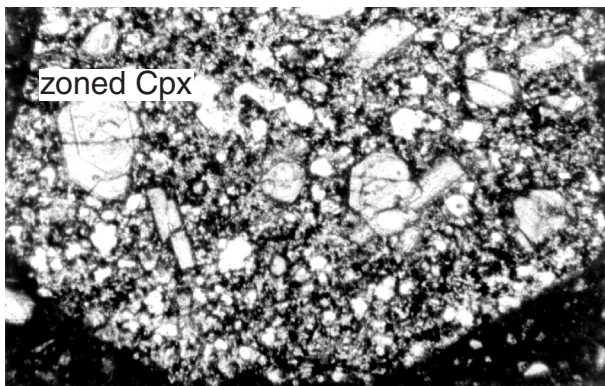
2



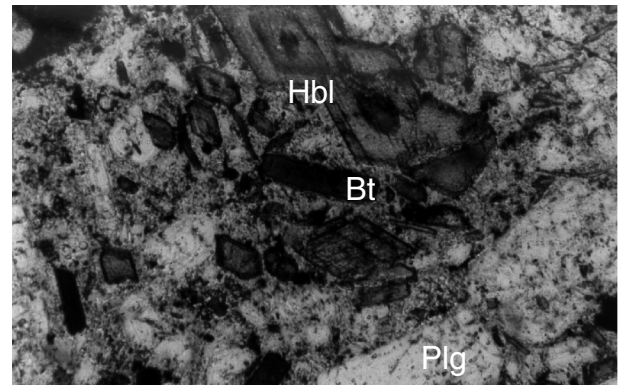
3



4

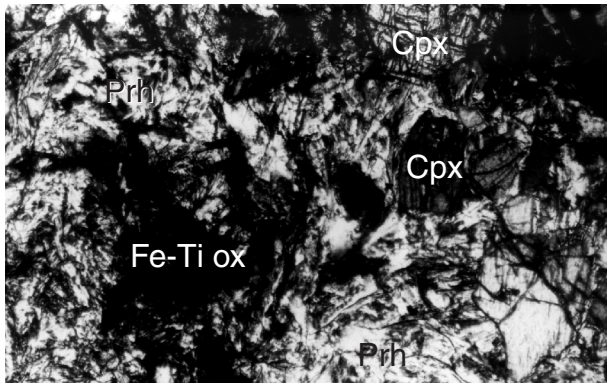


5

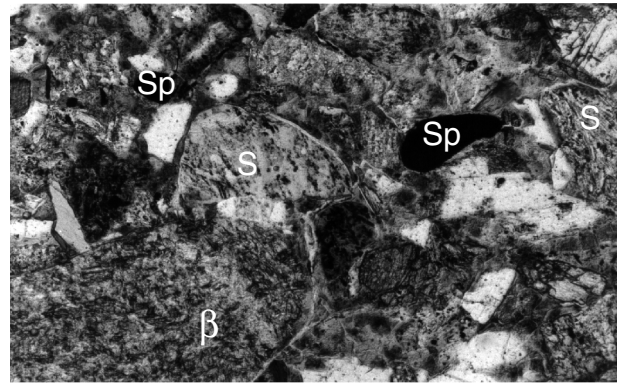


6

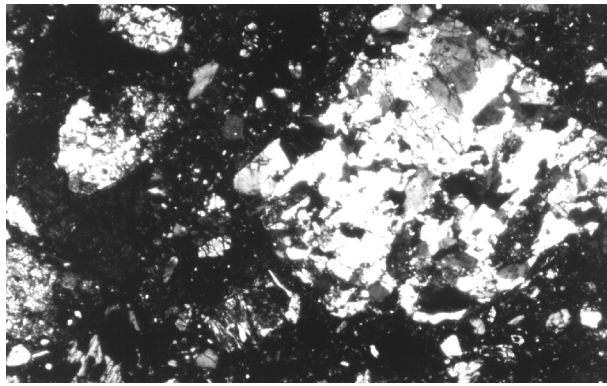
Plate P3. Optical photomicrographs. 1. Fine-grained Fe-Ti oxide gabbro. The plagioclase is pervasively altered to prehnite (Sample 180-1116A-6R-1, 37–39 cm; plane-polarized light; scale bar = 0.1 mm). 2. Polygenetic arenite: rounded clast of basalt, serpentinite clasts with net (center) and ribbon (right) textures, red spinel, and volcaniclastic fragments from calc-alkaline explosive activity (Sample 180-1108B-36R-1, 82–86 cm; plane-polarized light; scale bar = 0.5 mm). 3. Arenite including clasts of gneissic rock (left), epidosite, and lavas (Sample 180-1116A-6R-1, 37–39 cm; crossed polars; scale bar = 0.5 mm). 4. Dolerite altered to prehnite by metasomatism. Prehnite also fills the veins and replaces plagioclase. The clinopyroxene is largely preserved (Sample 180-1116A-6R-1, 37–39 cm; plane-polarized light; scale bar = 0.5 mm). 5. Fine-grained olivine-pyroxenite. Olivine (and plagioclase?) are altered to serpentine and chlorite (Sample 180-1116A-6R-1, 37–39 cm; plane-polarized light; scale bar = 0.5 mm). 6. Clast of calc-alkaline basaltic andesite. The phenocrysts are clinopyroxene and olivine. The groundmass shows plagioclase microliths and a clinopyroxene nodule (Sample 180-1115C-37R-CC, 1–3 cm; plane-polarized light; scale bar = 0.1 mm). β = basalt, Cpx = clinopyroxene, Phr = prehnite, S = serpentinite, Sp = spinel.



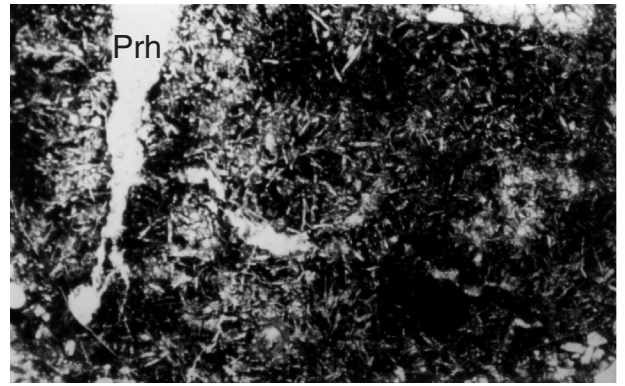
1



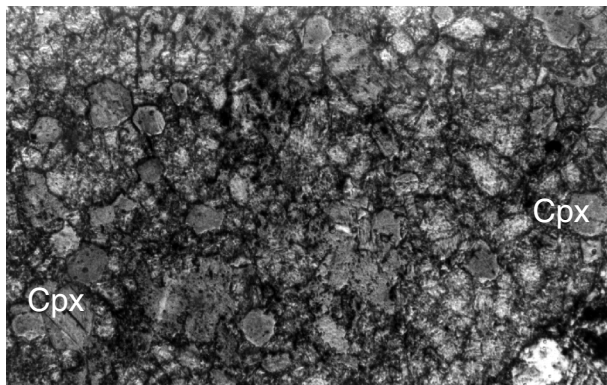
2



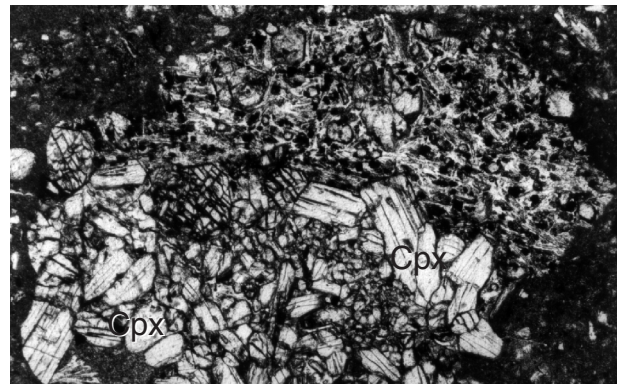
3



4



5



6

CHAPTER NOTES*

- N1. 19 February 2002—Lackschewitz, K., Bogaard, P.V.D., and Mertz, D.F., 2001. $^{40}\text{Ar}/^{39}\text{Ar}$ ages of fallout tephra layers and volcanoclastic deposits in the sedimentary succession of the western Woodlark Basin, Papua New Guinea: the marine record of Miocene–Pleistocene volcanism. *In* Wilson, R.C.L., Whitmarsh, R.B., Taylor, B., and Froitzheim, N. (Eds.), *Non-volcanic Rifting of Continental Margins: Evidence from Land and Sea*, Spec. Publ.—Geol. Soc. London, 187:373–388.
- N2. 19 February 2002—Robertson, A.H.F., Awadallah, S., Gerbaudo, S., Lackschewitz, K.S., Monteleone, B., Sharp, T.R., and other members of the Shipboard Scientific Party, 2001. Evolution of the Miocene–Recent Woodlark rift basin, SW Pacific, inferred from sediments drilled during Ocean Drilling Program Leg 180. *In* Wilson, R.C.L., Whitmarsh, R.B., Taylor, B., and Froitzheim, N. (Eds.), *Non-Volcanic Rifting of Continental Margins: A Comparison of Evidence from Land and Sea*, Spec. Publ.—Geol. Soc. London, 187:335–372.

*Dates reflect file corrections or revisions.